CdS-based photocatalyst for the Conversion of Formic acid to H_2

A dissertation submitted to the Department of Chemistry, Quaid-i-Azam University, Islamabad, in partial fulfillment of the requirements for the degree of

Master of Philosophy
In
Inorganic/Analytical Chemistry

By

Mr.Jamal Abdul Nasir

Supervised by

Dr. Zia-ur-Rehman

Department of Chemistry
Quaid-i-Azam University
Islamabad, Pakistan
(2014–2016)

In the name of Allah, the most beneficent, the most merciful

Dedicated to

To my parents

And

Supervisor

Dr. Zia Ur Rehman

"When parents and teachers work together well, everyone wins."

ACKNOWLEDGEMENTS

All praises for the ***Almighty Allah***, Who guides us in darkness and helps us in difficulties, Who has bestowed man with intelligence, wisdom and knowledge, and all respects to ***Holy Prophet Hazrat Muhammad*** (Peace be upon him) who exhorted his followers to seek for knowledge from cradle to grave and who enable us to recognize our creator.

I would like to express my sincere gratitude to my supervisor **Dr. Zia-ur-Rehman**, for giving me the opportunity to conduct this study and also for his help and continuous guidance throughout this research work.

Thanks to **Azam khan, Faisal hayat, Kashif, Noor-u-din, Imran Majeed, Ishtiaq bhai, Ibrar ahmad, Umair shamraiz, Hina Ambareen, Mehwish Arshad, Rabbia, Nida, Wagma, Maria, Nafeesa, Asma, Noor, and Mehwish,** for their valuable help and encouragement during my research. Without their assistance none of this would have been possible.

At last, but not least, my thanks go to all my dear friends in one or another way helping me in my study period, predominantly ***Samin*** *(my childhood friend),* ***Akhtar Munir, Zahid Nawaz Khattak, Imran Khan, Noor-u-din*** *and* ***Ibrar Ahmad*****.**

Special thanks are going to my family especially to my learned and zealous ***Father***, ***Greater Mother***, my siblings, all of my cousins especially **Rauf khan**, and **Junaid khattak** for their unlimited patience, cordial prayers and support which gave me confidence to complete this difficult work.

May ***Almighty Allah*** shower his limitless blessings and prosperity on all those who assisted me in anyway during completion of this work.

(**Jamal Abdul Nasir**)

Contents

List of tables

List of figures

Abstract

Cadmium dithiocarbamate complexes of $M(L)_2$ type were synthesized by reacting two different sodium salts of dithiocarbamate with $Cd(NO_3)_2.4H_2O$ (where L_1= Sodium dibutylcarbamodithioate and L2= Sodium 4-chlorobenzyl(benzyl)carbamodithioate). The synthesized complexes and ligands were characterized by NMR spectroscopy. The synthesized complexes were used as single source precursor for the synthesis of CdS nanoparticles by simple reflux method with ethylenediamine and octylamine as thermalizing solvent. The CdS nanoparticles were characterized by UV-Visible spectroscopy, XRD, FTIR, SEM and EDX and evaluated as a photocatalyst for decomposition of formic acid into hydrogen gas. The photocatalytic activity was remarkably enhanced by employing inexpensive co-catalysts e.g. $NiCl_2.6H_2O$, and $CoCl_2.6H_2O$ in photocatalytic decomposition of formic acid. The hydrogen production of 16.4±2.2 $mmolH_2h^{-1}g^{-1}$ and 25.1±4.2 $mmolH_2h^{-1}g^{-1}$ was observed for Nickel and Cobalt as a co-catalyst respectively. Further improvement was observed in the activity due to synergetic effect by adding both co-catalyst (dual) simultaneously to the reaction mixture of CdS-SF/FA, resulting in 27.5±5.1 $mmolH_2h^{-1}g^{-1}$ hydrogen production. H_2 production was sustained for more than 12 hour with turnover numbers greater than 2×10^3 for CdS/Co-Ni and 1.5×10^3, 1×10^3 for CdS/Ni, and CdS/Co respectively.

Keywords: Nanoparticles; cadmium sulfide; photocatalysis; inexpensive co-catalyst; Hydrogen production

Chapter 1

Introduction

1.1. Background

Due to increase in world population growth and the development of technologies that depend on fossil fuels, assets of fossil fuel ultimately will not be able to fulfil energy demand. Energy experts emphasize that reserves are less than 40 years for gasoline, 60 years for natural gas and 250 years for coal, that is a very big challenge for worldwide energy experts [1, 2]. The costs of fossil fuels are thus expected to increase in the near future. This will allow renewable energy sources such as solar, wind, hydrogen, etc. to be applied. Global production of CO_2 emission to decrease the risk of climate change e.g. greenhouse effect, requires a major rearrangement of the energy system. The use of hydrogen as an energy carrier is a long term option to reduce CO_2 emissions [3].

Using fossil fuels for energy needs in turn have adverse effects of environment throughout the world. There is an urgent need to speed up the process of employing the hydrogen Economy. The ideal endpoint for conversion to the Hydrogen Economy is the replacement of clean hydrogen for the present fossil fuels. The production of hydrogen from non-polluting sources e.g. solar energy is the supreme way [4]. Many environmental advantages can boom within the Hydrogen Economy, and as such, it can be mentioned as the Hydrogen Environmental Economy [5].

The use of solar quantum and thermal photons appears to be very efficient in the future work for hydrogen production. As solar hydrogen is not an energy, but an energy carrier that enables worldwide fulfilment of energy crisis. These studies point out that the role of hydrogen energy will become progressively important, with many researchers relating how world energy systems may go through a transition to a period in which the main energy carriers are hydrogen and electricity [6].

1.2. Technological Challenges

Formic acid to be used as a hydrogen storage material, should be decomposed by means of dehydrogenation ($HCOOH \rightarrow H_2 + CO_2$) instead of via dehydration ($HCOOH \rightarrow H_2O$ + CO) process, such that almost CO-free hydrogen is produced. This is mainly important

for direct uses in fuel cells because even a little amount of CO (100 ppm) in hydrogen feedstock can severely damage the Pt-based catalysts that are typically used as anodes of fuel cells. Consequently, we need to discover catalyst materials that are not only active for formic acid decomposition, but also have a good selectivity (selectively catalyzing the dehydrogenation reaction). But problem with CdS materials is its photocorrosion due to attack of the freshly generated holes, and then its solubility in aqueous medium.

Moreover, recombination of electron and hole and their suppression is also a big challenge. Semiconductors are described by two types of mobile carriers, electrons and holes in the conduction band and in the valence band respectively. These bands are separated by the energy gap i.e. 2.2eV to 2.7eV in case of CdS semiconductor. There is a continuous transition of electrons between the two bands. Loss of energy happen by electron drops from the conduction band into the valence band, a recombination process occurs and an electron hole pair vanishes. The energy of recombination will be appeared as a photon of light.

1.3. Statement of the problem

Even though TiO_2 has been the most successful photocatalyst till date, its biggest disadvantage is its wide band gap. The community is on a constant lookout for new materials with narrow band-gap which can harvest the visible photons (~65% of the sunlight). A recent scientific paper reported that cadmium sulphide would have excellent photocatalytic activities that may be useful for decomposition of organic compounds as titanium dioxide nanoparticles do, [7, 8]. As already mentioned that the problem with CdS is its photo instability. Which is due to photocorrosion of photo generated holes ($CdS + 2h^+ \rightarrow Cd^{2+} + S$). Photocatalyst in this case tend to be oxidized [9, 10]. This problem of photocatalyst might be overcome by loading with oxidation co-catalyst e.g. $CoCl_2.6H_2O$. Gradual oxidation of co-catalyst in turn result in efficient removal of photo generated holes from the photocatalyst and thus semiconductors are being sheltered from photo-oxidation.

Furthermore, recombination problem is overcome by the loading of dual co-catalyst. Loading of suitable dual co-catalyst on photocatalyst has been proved to be very efficient in increasing the photocatalytic activities of semiconductor. Dual co-catalysts are necessary for developing highly efficient photocatalyst for photocatalytic hydrogen

production [11, 12, 13]. Dual co-catalysts for reduction and oxidation was recently developed as an effective co-catalyst for the remedy of oxidation of CdS particles as well as for suppression of recombination phenomenon [10]. $CoCl_2.6H_2O$ as a oxidation co-catalyst and $NiCl_2.6H_2O$ as a reduction co-catalyst have been used on CdS semiconductor and shows synergic effect just after 6 hours photocatalysis by efficiently increase in H_2 production . Loading of dual co-catalyst is supposed to be beneficial for effective suppression of electron-hole recombination. Single metal Ni and Co catalysts were also very effective, but it was observed after comparative study that they were inferior to Ni–Co catalyst, all in terms of conversions of formic acid, suppression of recombination and selectivity.

Selectivity was also controlled by addition of aqueous dispersed solution of catalyst, because water act as a co-catalyst by lowering the activation barrier in favor of decarboxylation pathway to be followed **(shown in figure 1.1 and 1.2).**

In view of all the achievements made in catalyst development, using formic acid as a hydrogen storage material appears to be a sustainable technology that deals with many benefits as compared to the conservative hydrogen storage technologies. Still, it is important to note that the catalyst materials developed up to now are almost totally dependent upon expensive elements act as a catalyst and co-catalyst e.g. Au, Pd, Pt, on the surface of CdS nanoparticles may not allow energy experts to commercialize this technology as an alternate energy source for future fuel cell. To commercialize this technology, we are still in need of innovative catalyst materials that are not only active and selective for formic acid decomposition but also potentially inexpensive [14]. Such inexpensive co-catalyst loading on CdS nanoparticles with high activity may greatly encourage the practical application of formic acid as a hydrogen storage material.

Therefore, the present work focused on investigation of cadmium sulphide nanoparticles loading with non-noble co-catalyst for selective decomposition of formic acid into hydrogen gas. In this article, current achievements in the development of catalysts for formic acid decomposition has been discussed, particularly focusing on using heterogeneous inexpensive catalyst and co-catalyst systems.

1.4. Objective of the study

We aimed to prepare CdS nanoparticles and explore their potential use in photocatalytic process. Particularly, the study aimed to

i. Study the effects of some parameters that may affect the size, phase, and stability of nanoparticles during photocatalytic process.
ii. Effects of different co-catalyst on photocatalytic decomposition of formic acid into hydrogen gas.
iii. Explore various chemical reduction methods as possible synthesis methods for CdS nanoparticles.
iv. Characterize the produced CdS nanoparticles, and find out their stability factor before and after photocatalytic process by various means i.e. XRD, SEM, EDX, UV-Visible, and FTIR
v. Evaluate the photocatalytic activity of the produced CdS nanoparticles toward hydrogen production.
vi. Decrease in global anthropogenic carbon dioxide (CO_2) emissions and increase local (urban) air quality.
vii. Ensure safety of energy supply.
viii. Create new, safe and clean industrial and technological energy base processes, essential for our economic prosperity [15].
ix. There should be renewable forms of energy so that future generations do not face energy crisis problems.
x. They must not expose greenhouse or pollutant gases so that current and future generations do not inherit an uninhabitable planet [14].

1.5. LITERATURE REVIEW

1.5.1. Natural Sources of Formic Acid

Natural sources of formic acid comprise ant venom and vegetation releases of hydrocarbons that are photo-oxidized by various means to organic acids [16, 17].

1.5.2. Commercial Production and Synthesis of Formic Acid

Because of many applications of formic acid, most particularly hydrogen storage in liquid phase, commercial synthesis of this simple carboxylic acid has faced significant increase in the past periods. These commercial methods for production of formic acid include:

i. Reaction of formates with strong mineral acids
ii. Hydrolysis of methyl formate
iii. Hydrolysis of formamide
iv. By-product oxidation of hydrocarbons to acetic acid
v. Catalytic hydrogenation of CO_2
vi. Conversion of bio-based carbohydrates to formic acid using molecular oxygen
vii. By-product conversion of glucose to Levulinic Acid

1.5.3. Applications of Formic Acid

Physical properties of formic acid clearly indicate that it is a safe source of hydrogen. It is liquid at room temperature and is thus an easy-to-handle storage material although it corrodes the skin [18]. As hydrogen is considered one of the most significant energy flight path for its applications in the fuel cell technology, formic acid is also drawing attention by holding hydrogen. Moreover, without being decomposed to yield hydrogen to be used in proton exchange membrane (PEM) fuel cells [19]. Formic acid is also used in leather and textile trades for tanning and dyeing and also it is used up in silages. In 1998, as reported by BASF, 35% of the industrial formic acid was used in silages, while 25% was used in textiles and leather industry, and the other 40% was shared in pharmaceuticals, crop protection agents, latex and rubber auxiliaries and miscellaneous uses [20].

1.5.4. Why Hydrogen as an energy carrier?

Hydrogen is expected to play an important role in future energy developments. The primary factor that will determine the definite role of hydrogen will in the cards to be energy demand. Hydrogen is expected in the future to substitute fossil fuels and to become the favoured portable energy carrier for vehicles.

Currently 500 billion functioning as of hydrogen, equating to about 6.5 eV of energy, are produced per annum worldwide. Approximately, 99% is produced from fossil fuels, mostly by steam reforming of natural gas [21]. It is likely to produce hydrogen using other production methods and different energy sources. As the depletion of fossil fuels and the growing adverse effect of these fuels on environment, researcher are now investigating

fuels which are renewable and environmental friendly [22]. There is a rising alertness globally that hydrogen is the fuel of the future. While hydrogen can be generated using different processes, only some of them are environmental friendly. It is debated that hydrogen generated from water and organic compounds using solar energy, is a leading candidate for a renewable and environmentally safe energy carrier due to the following reasons [14].

i. Solar-hydrogen technology is relatively simple and, therefore, the cost of such a fuel is expected to be substantially less than that of the present price of gasoline.

ii. The raw material for the production of solar-hydrogen are water, and formic acid, which is a renewable resource. The resultant climate change in the form of global warming and greenhouse effect is forcing us to say good bye to this fossil heritage and look to new sources of energy like hydrogen economy.

1.5.5. Photocatalytic decomposition of formic acid

FA can be catalytically decomposed to H_2 and CO_2 through a dehydrogenation pathway.

$$HCOOH \rightarrow H_2(g) + CO_2(g) \quad (1.1) \quad \Delta G = -48.4 \text{ kJ/mol}^{-1}$$

However, carbon monoxide (CO), which is a serious poison to catalysts of fuel cells, can also be generated through a dehydration pathway.

$$HCOOH \rightarrow H_2O + CO(g) \quad (1.2) \quad \Delta G = -28.5 \text{ kJ mol}^{-1}$$

Depending on the catalysts, pH values of the solutions, as well as the reaction temperatures [23, 24]. Recently, much progress has been made on the heterogeneous catalysis for the selective dehydrogenation of FA. However, the thermodynamic and kinetic properties of FA dehydrogenation, especially without any extra additive, still need to be further promoted. More importantly, all the reported heterogeneous catalysts up to now only consist of noble metals, including, for example, Pd, Au, Ag, and Pt, which greatly hinders their large-scale practical applications because of their high costs and low reserves in the earth crust [23]. CdS shows considerable interesting application in catalytic photodecomposition of formic acid into hydrogen gas. Formic acid, containing 4.4 Wt. % hydrogen, needs to be decomposed to convert to molecular hydrogen as a by-product [25]. Formic acid decomposes by two different pathways: decarboxylation **(Eq. 1.1)** and decarbonylation (hydration) **(Eq. 1.2).** The earlier, also called dehydrogenation, produces

hydrogen and carbon dioxide, while the latter, also called dehydration, produces CO and H_2O. Both reactions are exergonic reaction with ΔG of -48.4 kJ mol^{-1} and -28.5 kJ mol^{-1} for R.1 and R.2 respectively [26].

1.5.5.1. Selectivity

Decomposition of formic acid, the simplest carboxylic acid has been studied both experimentally and theoretically. Although many mechanisms have been suggested in the literature, including free-radical chemistry, ionic chemistry, surface catalysis, and molecular elimination is considered the most important mechanism in both gas phase [31, 29, 30] and in aqueous phase [27, 28]. It is generally agreed that the reaction network consists of two parallel pathways **(Eq. 1.1, 1.2)**.

The thermal decomposition of formic acid into CO and H_2O, which depends on the temperature and the formic acid concentration, becomes no negligible at high temperature [32]. Formic acid can be catalytically decomposed on mandate to regenerate H_2 and CO_2 equation (1) [33, 34]. The aqueous phase experiment shows the main decomposition pathway is decarboxylation due to larger CO_2 yield compared to CO. On the other hand, the dehydration decomposition pathway is more promising than decarboxylation in the gas phase experiments [29].The reason for this could be clarified by the higher activation energy necessary for the decarboxylation reaction in the absence of water molecules **(Figure 1.1)** [35]. Water decreases the activation barrier and acts as a homogeneous catalyst in decomposition of formic acid **(Figure 1.2)** [29].

The main assumptions of this work may be summarized briefly as follows:

i. The activation barriers for the decomposition of monomeric formic acid to H_2 plus CO_2 and to H_2O plus CO are very similar. The best estimates for the decarboxylation and dehydration activation energies are ~ 71 and ~ 68 kcal mol^{-1}, respectively.

ii. The barrier height for the 1, 2-hydrogen shifts from formic acid to dihydroxymethylene is somewhat higher than those for the molecular dissociations. The best estimated barrier is ~ 79 kcal mol^{-1}. These predicted barriers from higher level theory are in general agreement with earlier *ab initio* studies [36, 37] and with very recent research by Francisco [38]. Experimental reinvestigation of the thermal reactivity of formic acid would be valuable.

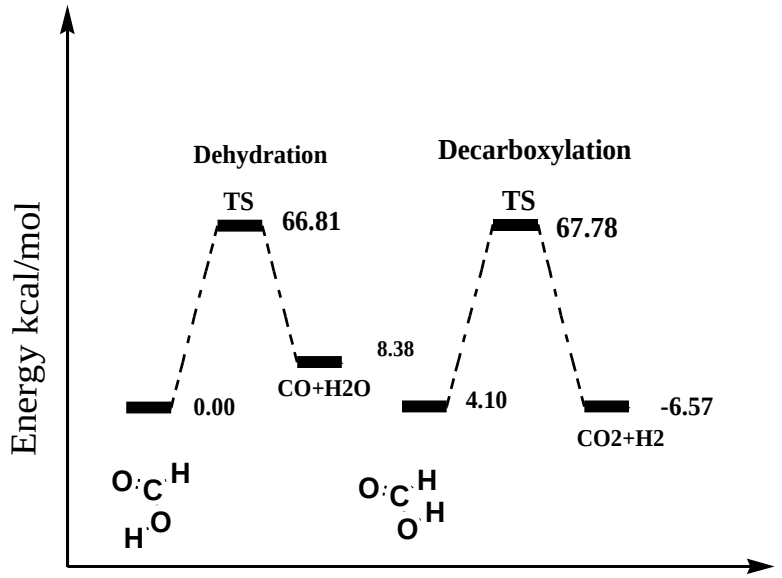

Figure 1.1: Energy diagram for formic acid decomposition in the absence of water.

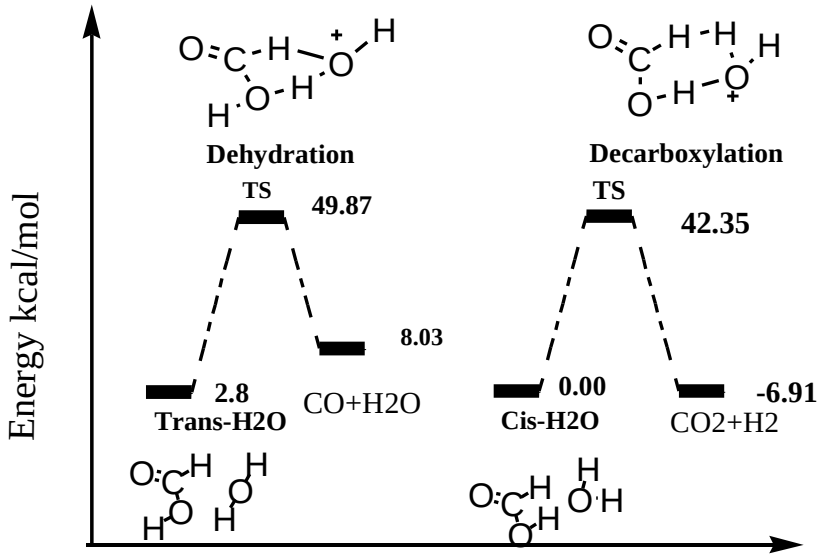

Figure 1.2: Energy diagram for formic acid decomposition assisted in the presence of water molecule.

The adding of water molecules to formic acid solution and the transition-state structure, pull down the activation barriers for both dehydration and decarboxylation, as shown in **(Figures 1.1** and **1.2).** Water acts as a co-catalyst for both decomposition pathways by changing the transition states, but the decarboxylation transition state is lower in energy than the dehydration transition state for both water-assisted states, which shows that decarboxylation is the favoured decomposition path in the presence of water. This tendency is reliable with the experimental observation that decarboxylation is the

foremost pathway for decomposition of formic acid [39, 40]. This work also focus on evolution activity of hydrogen as well as selectivity **Table 1.1).**

Table 1.1 Comparison of selected literature photocatalysts for FA-to-H_2 conversion at room temperature.

Catalyst	H_2 activity[a] /mmol H_2 $g_{catalyst}^{-1}h^{-1}$	Selectivity[b] [%]	EQY [%]	Light(nm)	Life time [h]	Ref
$RuCl_2(C6H6)]_2$ + 12 PPh_3	153.9	n/a	n/a	>380	5	**[50]**
$HCo[(PPh(OEt)_2]_4$	0.59	n/a	n/a	>275	6	**[51]**
Co_3O_4-$LiNbO_3$	0.78	n/a	n/a	200-600	2.5	**[52]**
$Fe_3(CO)_{12}/PPh_3$/tpy	2.7	"trace CO"	n/a	>385	24	**[53]**
Bulk CdS	0.078	n/a	n/a	>400	12	**[54]**
CdS-TNT TiO_2	0.56	n/a	5.1	>430	8	**[55]**
Pt-CdS	1.84	n/a	20 (470 nm)	>320	10	**[56]**
Pt-CdS	0.85	83	n/a	>400	20	**[57]**
Pt-CdS NR	4.46	n/a	13.9(400-700 nm)	>420	50	**[58]**
CdS-NR	0.22	n/a	n/a	>420	n/a	**[59]**
Pt-CdS-QD	1.22	n/a	21.4(420 nm)	>420	30	**[60]**
Pt-CdS@Al-MHS	0.31	n/a	2.0 (420 nm)	>420	6	**[61]**

Catalyst	**H_2 activity[a] /mmol H_2 $g_{catalyst}^{-1}h^{-1}$**	**Selectivity[b] [%]**	**EQY [%]**	**Light(nm)**	**Life time [h]**	**Ref**
CdS@Al-HMS	0.13	n/a	n/a	>420	6	**[63]**
CdS/ZnS NP	1.24±0.02	n/a	n/a	>420	40	**[64]**
Ru-CdS/ZnS NP	5.85±0.09	n/a	20	>420	40	**[65]**
CdS-TNT + WO_3	0.619	n/a	n/a	>420	3	**[66]**
Pt-CdS-TNT	4.26	n/a	n/a	>420	3	**[67]**
hydrogenase-CdS	0.356	20	3.1 (IQE)	400-600	3.5	**[68]**
CdS	0.036	3.2	1.9 (IQE)	400-600	3.5	**[69]**
QD-MPA	52.1±6.6	98.8±0.1	n/a	AM1.5G >420	>168	**[70]**
QD-MPA/$CoCl_2$	116±14	99.4±0.1	21.2±2.7 (460 nm)	AM1.5G >420	>168	**[70]**
QD-MPA/$CoCl_2$	218±22	98.9±0.1	n/a	AM1.5G	>24	**[70]**
Pd@C_3N_4	53.4	100	n/a	>400	6	**[41]**
Pd@Au-NRs	10	100	n/a	>460 , 1 sun	n/a	**[42]**
AuPd-TiO_2 NW	17.7	99.7	15.6 (365 nm)	AM1.5, 1 sun	9	**[43]**

Au-TiO_2 NW	3.9	90.7	8.1 (365 nm)	AM1.5, 1 sun	9	**[43]**
Pd-TiO_2 NW	10.9	98.2	11.6 (365 nm)	AM1.5, 1 sun	9	**[43]**
TiO2 NW	0.80	69.6	0.35 (365 nm)	AM1.5, 1 sun	9	**[43]**
Pd-Si	1.1	100	n/a	Visible	5	**[44]**
Pt-Si	0.001	n/a	0.02 (633 nm)	>390 , 2 sun	100	**[45]**
Pt-TiO_2	1.62	n/a	n/a	UV	10	**[46]**
Pt-(CuIn)0.2Zn1.6S_2	Cu-TiO2	n/a	n/a	>420	4	**[47]**
Rh-N:TiO_2	153.9	98	n/a	230-440	4	**[48]**
Cu-TiO_2	0.59	n/a	n/a	UV	5	**[49]**
CdS/Ni-Co	**27.5 ±5.1**	**99.6**	**15.52 (460 nm)**	**AM1.5G >420**	**>24**	**This work**
CdS/$CoCl_2$	**16.4 ±2.2**				**>24**	**This work**
CdS/$NiCl_2$	**25.1 ±2.3**				**>24**	**This work**

1.6. Nanoparticles

The term nanoparticle (NP) refers to particles with sizes between 1 and 100 nm that show unusual properties compared to the corresponding bulk materials. This is because nanoparticles have a large surface area, a greater segment of surface atoms and a high surface to volume ratio in contrast to their bulk counterparts. As the size of a nanoparticle decreases, the fraction of surface atoms increases, subsequently it increases the reactivity and makes them highly reactive catalysts [71, 72, 73]. It is careful for companies to try to mitigate the potential risks of nanoparticles during the design stage rather than downstream during manufacturing or customer use [74].

Several factors can mark the properties of nanoparticles. Among these, size (diameter, length, width, etc.), surface (surface chemistry, surface charge, surface morphology, surface roughness, and surface contamination), and structure of the nanoparticles (crystal structure, shape, porosity, chemical composition, aggregation, etc.) are the major characteristics that determine their fundamental properties such as color, melting point, conductivity, and reactivity. Nanomaterial form a recent area of intense scientific attention because nanoscale materials show unique properties and have an extensive variety of applications in the development of magnetic materials for data, medical diagnostics, photocatalyst , sensors, and for hydrogen economy [75, 76, 77]. Potential applications of nanotechnologies have been examined in some important sectors, such as energy, communications, water purification, pollution reduction and environmental progress, medical and biomedical applications. This technology allows substantial reduction of resource intake and pollution via improving the sustainability of energy utilization, recycling and detoxification technology [78, 79].

Heterogeneous photocatalysis using nano-semiconductor has become the most compelling technology, because it can fully catalyze and degrade various organic and inorganic substances in air and wastewater [80, 81] for example, TiO_2 photocatalyst has received much attention for the past several decades, especially in water treatment technology. However, because of the large band gap of TiO_2 its practical application is limited due to the need of an ultraviolet excitation source [82]. Meanwhile, owning to the narrower band gaps and more negative potentials of conduction bands of CdS [83, 84], they have also been applied to the photocatalytic reduction of CO_2 and production of hydrogen for future fuel cell technology [95, 83, 85] etc. CdS is one of the most well-known photo-catalyst used for photocatalytic decomposition of water and formic acid thus helping in overcoming the greenhouse effect [86, 87]. Wide band gap semiconductors are the most suitable photocatalysts for CO_2 photoreduction, because they provide sufficient negative and positive redox potentials in conduction bands and valence bands, respectively. The disadvantage of using wide band gap semiconductors is the requirement for high energy input. Semiconductors with narrow band gap, like cadmium sulfide (CdS, 2.4 eV) work in the visible range, but it is not sufficiently positive to act as an acceptor. This causes the photocatalyst to decay with the holes formation and being photocorroded. A good

catalyst should produce a single chemical product at high rates that compete with electron-hole recombination [88]. In addition, cadmium sulfide (CdS) with narrow band gap (2.42 eV) was always combined with TiO_2 (TiO_2/CdS heterostructure) to reveal the enhanced photocatalytic ability under visible light [89, 90].

1.6.1. Types of nanoparticles

Nanoparticles categorized as engineered nanoparticles (ENPs) and non-engineered nanoparticles (NENPs). Non-engineered nanoparticles present in the environment derive from natural events such as terrestrial dust storms, erosion, volcanic eruptions, and fires [91, 92]. Engineered nanoparticles (ENPs) are intentionally produced by man using many different materials, such as metals (including Ag, Zn, Au, Ni, Fe, and Cu) [93] metal oxides (TiO_2, Fe_3O_4, SiO_2, CeO_2, and Al_2O_3). Engineered NPs are used for special purposes. Their origin can be biological, like lipids, phospholipids, and lactic acid, or chemical, such as carbon, silica and various metals. On the other hand, NENPs are formed in undesired ways such as particles emitted as a byproduct, for example, in the combustion of fuels [94]. On the basis of chemical composition, nanoparticles can be classified as carbon-based and inorganic nanoparticles. Carbon-based materials are fullerenes, carbon nanotubes etc. while inorganic nanoparticles can further be categorized as metal oxides [zinc oxide, iron oxide, titanium dioxide, etc.], metals [gold, silver, iron, etc.] and quantum dots (QD) [cadmium sulfide, cadmium selenide, etc.]. There have been a variety of developments in QD synthesis and characterization over the past two years [95]. On the basis of dimensionality nanoparticles are categorized into the four groups, these are; 0D nanoclusters, 1D multilayers, 2D nanograined layers, and 3D-equiaxed bulk solids [96]. One-dimensional nanostructures (nanorods, nanowires, nanotubes, and nanobelts) have their unique electronic, optical and mechanical properties and have potential applications in both fundamental research and fabricating nanodevices [97]. Nanoparticles formed from amphiphilic block copolymers include micelles, nanospheres, nanocapsules, and polymersomes [98], while polymeric nanoparticles are colloidal structures composed of synthetic or semi synthetic polymers. Nanocapsules are systems in which the drugs is confined to a cavity surrounded by a unique polymer membrane, while nanospheres are matrix systems in which the drug is physically and uniformly dispersed [99].

1.6.2. Synthesis of nanoparticles

Nanoparticles may be synthesized using various starting materials by different physical and chemical methods, with the produced particles differing in elemental composition, shape, size, and chemical or physical properties [100]. These methods can generally be categorized as "top-down" and "bottom-up" [74, 101, 102]. The top-down synthesis concerns the production of nanostructured materials by size reduction of a very big solid material into smaller, nano-sized portions, from a suitable starting material [10]. Size reduction may involve various physical and chemical treatments, such as mechanical milling, chemical etching, thermal ablation, laser ablation, and explosion processes. The major drawback of the "top-down" method is the introduction of imperfections in the surface structure of the product. In the ''bottom-up'' synthesis, the nanostructure should be arranged atom-by-atom, layer-by-layer to build the nanoscale structures from their atomic and molecular constituents either by chemical or biological procedure(s) [102].

1.6.3 Synthesis of CdS nanoparticles

A well-designed synthesis method needs to control the factors that determine the properties of nanoparticles such as sizes, shapes, surface, and composition. Some of these factors are types and concentrations of stabilizing agents, initial concentrations of precursor chemicals, reaction temperature, time, and pH. CdS nanostructures by several methods such as electrochemical synthesis [103, 104], chemical synthesis [105], solvothermal route [106], thermal evaporation [107], chemical vapor deposition [108], vapor–liquid–solid growth [109] etc. Beside this, several approaches have been used for nanowire fabrication using chemical etching technique. Ling-min et al. [110] have synthesized CdS/SiO_2 nanowire arrays and CdS nanobelts by thermal evaporation of mixture of CdS and CdO powders with highly selective etching occurring on the silicon substrate surfaces [111] have created unique diameter-modulated GaN nanowires by reacting the wires of different diameters with 1M hydrochloric acid (HCl). Using seed-mediated growth approach Sajanlal and Pradeep [112] have converted gold nanoparticle into nanowire and nanoplate at certain cetyltrimethylammonium bromide (CTAB) concentration in the presence of ascorbic acid [113] have also reported that silver nanorods and nanowires can be successfully synthesized by converting nanoparticles at a relatively

low temperature of 50 °C. Recently prepared CdS nanowire by chemical bath deposition (CBD) using porous anodic aluminum oxide (AAO) template [114]. In first step films of CdS nanoparticle were prepared by CBD. The nanoparticle films were transformed into fibril-like nanowire using chemical etching in second step [115]. GMA-IDA chelating groups within the copolymer were the coordination sites for chelating Cd^{2+}, at which nanosized CdS nanocrystals were grown by the dry method (H_2S) and the wet method (Na_2S) [116]. Nanometer-sized CdS semiconductor particles were synthesized in the presence of sodium citrate, and successively surrounded by a homogeneous silica shell [117]. Mono disperse CdS nanorods are synthesized by Au nanoparticle catalyzed colloidal synthesis. Synthesis of CdS nanoparticles by anisotropic growth using organic solution and Au nanoparticles as catalyst in a high temperature.

1.7. Stabilization of CdS nanoparticles

A novel method for the stabilization of semiconductor particles is silica coating [118] have reported that silica covering leads to a 100-fold decrease in photocorrosion rates for CdS nanoparticles. Moreover, the silica coating opens up the prospect for controlled synthesis of photonic crystals [117]. The usage of silica shells as stabilizers, rather than organic molecules, has a number of benefits. Despite avoiding coagulation during chemical or electronic processes, the silica shells are probable to act as a passivant due to a disorderly amorphous structure [119]. Double-hydrophilic block copolymers comprising of a solvating poly (ethylene glycol) PEG block and a poly (ethylene imine) PEI binding block have been used as effective stabilizers for the solution mixture of high-quality CdS nanoparticles in water and methanol [120]. The encapsulation of CdS nanoparticles, restrained on thiol-modified polystyrene particles with polythiourethane has been examined. CdS stabilization can now carryout effectively, against photoirradiation, by encapsulation within polythiourethane, formed by means of 1, 2-ethanedithiol and m-xylene diisocyanate as monomers. The formed (PSt−CdS) PTU composite has been cast-off for photocatalytic H_2 generation from 2-propanol aqueous solution [121]. **Table 2** shows the comparison of some literature size controlled synthesis of CdS nanoparticles to this work.

Table 2: Some examples of size controlled synthesis of cadmium sulfide nanostructures

Structure	Reagent	Stabilizer	Advantages	References
Spherical and uniform	$Cd(NO_3)_2.H_20$ Na_2S	CTAB reverse micelles	Reflux treatment improve the optical properties	**[122]**
Nanorods and faceted nanop articles	cadmium ethylxanthate hexadecylamine (HDA)		Change of morphology at different temperature	**[123]**
well-resolved cubic structure and monodisperse in size	$CdCl_2$ and Na_2S	poly(ethylene glycol) PEG block and a poly(ethylene imine) PEI	good resistance against oxidation for months, according to their polymer shell	**[124]**
narrowest size	tetrabutylammonium hydrogen sulphide,water/sodium bis(2-ethylhexyl) sulfosuccinate/n-heptane, $CdSO_4$	bis(2-ethylhexyl)amine (BEA)	CdS nanoparticles can be easily separated from the reaction medium	**[125]**
spherical-shaped, rods	$Cd(S_2CNEt_2)$, hexadecylamine (HAD	HAD acts as a shape-controlling ligand but also as a stabilizing ligand	varying the precursor concentration, and temperature, size and shape change	**[124]**
Transparent CdS nanocrystals	$CdCl_2$,Na_2S,2-Mercaptoethanol(ME)		At room temperatue, take only 20 minutes	**[125]**
Leaf and flower-like CdS nanocrystals	Ammonium thiocyanante and cadmium		Lowest formation temperature	**[126]**

Nanorods, multipods, and triangular	$Cd(CH_3COO)_{23}.2H_2O$, dodecylamine		Solvothermal time and precursor have fully control on morphology of nanocrystals	**[127]**
Small size and hexagonal shape CdS nanoparticles	Dithiocarbamate complex of cadmium, and ethylenediamine	No stabilizing agent	Good crystalinity, and photocatalyst	**This Work**
Small size and Cubic shape CdS nanoparticles	Dithiocarbamate complex of cadmium, and Octylamine	No stabilizing agent	Small size,	**This Work**

References

1. Midilli, A., I. Dincer, and M. A. Rosen. "The role and future benefits of green energy." International journal of green energy 4.1 (2007): 65-87.
2. Midilli, A., et al. "On hydrogen and hydrogen energy strategies: I: current status and needs." Renewable and sustainable energy reviews 9.3 (2005): 255-271.
3. Momirlan, Magdalena, and T. N. Veziroglu. "Current status of hydrogen energy." Renewable and Sustainable Energy Reviews 6.1 (2002): 141-179.
4. Zweig RM. Proceedings of the Ninth World Hydrogen Energy Conference. Paris (France), 1992:1995.
5. Harrison, Kevin, and Johanna Ivy Levene. "Electrolysis of water." Solar Hydrogen Generation. Springer New York, 2008. 41-63.
6. Midilli, Adnan, et al. "Solar hydrogen production from hazelnut shells."International journal of hydrogen energy 25.8 (2000): 723-732.
7. Sasikala, Rajamma, Archana R. Shirole, and Shyamala R. Bharadwaj. "Enhanced photocatalytic hydrogen generation over ZrO_2–TiO_2–CdS hybrid structure." Journal of colloid and interface science 409 (2013): 135-140.
8. Guo, Xingyuan, et al. "Enhanced near-infrared photocatalysis of NaYF 4: Yb, Tm/CdS/TiO 2 composites." Dalton transactions 43.3 (2014): 1048-1054.
9. Bao, Ningzhong, et al. "Self-templated synthesis of nanoporous CdS nanostructures for highly efficient photocatalytic hydrogen production under visible light." Chemistry of Materials 20.1 (2007): 110-117.
10. Yang, Jinhui, et al. "Roles of cocatalysts in photocatalysis and photoelectrocatalysis." Accounts of chemical research 46.8 (2013): 1900-1909.
11. Ma, Baojun, et al. "The synergistic effects of two co-catalysts on $Zn2GeO_4$ on photocatalytic water splitting." Catalysis letters 134.1-2 (2010): 78-86.
12. Maeda, Kazuhiko, et al. "Photocatalytic overall water splitting promoted by two different cocatalysts for hydrogen and oxygen evolution under visible light." Angewandte Chemie 122.24 (2010): 4190-4193.
13. 林峰, et al. "Photocatalytic oxidation of thiophene on $BiVO_4$ with dual co-catalysts Pt and RuO_2 under visible light irradiation." (2012).

14. Nowotny, J., et al. "Solar-hydrogen: environmentally safe fuel for the future."International journal of hydrogen energy 30.5 (2005): 521-544.

15. Edwards, Peter P., et al. "Hydrogen and fuel cells: towards a sustainable energy future." Energy Policy 36.12 (2008): 4356-4362.

16. Hoffman, Donald R. "Ant Venoms." Current Opinion in Allergy and Clinical Immunology 10.4 (2010): 342-346.

17. Kavouras, Ilias G., Nikolaos Mihalopoulos, and Euripides G. Stephanou. "Formation of atmospheric particles from organic acids produced by forests."Nature 395.6703 (1998): 683-686.

18. Johnson, Tarn C., David J. Morris, and Martin Wills. "Hydrogen generation from formic acid and alcohols using homogeneous catalysts." Chemical Society Reviews 39.1 (2010): 81-88.

19. Azadi Manzour, Faraz. Catalytic Conversion of Biomass for the Production of Hydrogen; Decomposition of Formic Acid. Diss. 2014.

20. Drury, David J. "Formic acid." Kirk-Othmer Encyclopedia of Chemical Technology (2000).

21. Midilli, A., et al. "On hydrogen and hydrogen energy strategies: I: current status and needs." Renewable and sustainable energy reviews 9.3 (2005): 255-271.

22. Hydrogen: The Wonderful Fuel by T.N.Veziroglu F.berbir

23. Wang, Zhi-Li, et al. "An efficient CoAuPd/C catalyst for hydrogen generation from formic acid at room temperature." Angewandte Chemie International Edition 52.16 (2013): 4406-4409.

24. Loges, Björn, et al. "Kontrollierte Wasserstofferzeugung aus Ameisensäure-Amin-Addukten bei Raumtemperatur und direkte Nutzung in H_2/O_2-Brennstoffzellen." Angewandte Chemie 120.21 (2008): 4026-4029.

25. Enthaler, Stephan. "Carbon Dioxide-The Hydrogen-Storage Material of the Future?"ChemSusChem 1.10 (2008): 801-04.

26. Tedsree, Karaked, et al. "Hydrogen production from formic acid decomposition at room temperature using a Ag-Pd core-shell nanocatalyst."Nature nanotechnology 6.5 (2011): 302-307.

27. Melius, C. F., N. E. Bergan, and J. E. Shepherd. "Effects of water on combustion kinetics at high pressure." Symposium (International) on Combustion. Vol. 23. No. 1. Elsevier, 1991.

28. Goddard, John D., Yukio Yamaguchi, and Henry F. Schaefer III. "The decarboxylation and dehydration reactions of monomeric formic acid." The Journal of chemical physics 96.2 (1992): 1158-1166.

29. Akiya, Naoko, and Phillip E. Savage. "Role of water in formic acid decomposition." AIChE Journal 44.2 (1998): 405-415.

30. Akiya, Naoko, and Phillip E. Savage. "Role of water in formic acid decomposition." AIChE Journal 44.2 (1998): 405-415.

31. Yoo, Jong Suk. "Formic Acid as a Viable Hydrogen Storage Material."

32. Morris, David J., Guy J. Clarkson, and Martin Wills. "Insights into hydrogen generation from formic acid using ruthenium complexes." Organometallics28.14 (2009): 4133-4140.

33. Coffey, R. S. "The decomposition of formic acid catalysed by soluble metal complexes." Chemical Communications (London) 18 (1967): 923b-924.

34. Zhou, Xiaochun, et al. "High-quality hydrogen from the catalyzed decomposition of formic acid by Pd–Au/C and Pd–Ag/C." Chemical Communications 30 (2008): 3540-3542.

35. Francisco, J. S. "A comprehensive theoretical examination of primary dissociation pathways of formic acid." The Journal of chemical physics 96.2 (1992): 1167-1175.

36. Huang, Chun-Liang, Chen-Chang Wu, and Min-Hsiung Lien. "Ab Initio Studies of Decarboxylations of the β-Keto Carboxylic Acids XCOCH2COOH (X= H, OH, and CH3)." The Journal of Physical Chemistry A 101.42 (1997): 7867-7873.

37. Ruelle, P. "Ab initio study of the unimolecular pyrolysis mechanisms of formic acid: additional comments based on refined calculations." Journal of the American Chemical Society 109.6 (1987): 1722-1725.

38. Francisco, J. S. "A comprehensive theoretical examination of primary dissociation pathways of formic acid." The Journal of chemical physics 96.2 (1992): 1167-1175

39. Brill, T. B., et al. "Spectrokinetics of Solvo-Thermal Reactions." Proc. 2nd Int. Conf. Solvotherm. Reactions. 1996.

40. Yu, Jianli, and Phillip E. Savage. "Decomposition of formic acid under hydrothermal conditions." Industrial & Engineering Chemistry Research 37.1 (1998): 2-10.

41. Cai, Yi-Yu, et al. "Highly Efficient Dehydrogenation of Formic Acid over a Palladium-Nanoparticle-Based Mott–Schottky Photocatalyst." Angewandte Chemie 125.45 (2013): 12038-12041.

42. Zheng, Zhaoke, Takashi Tachikawa, and Tetsuro Majima. "Plasmon-Enhanced Formic Acid Dehydrogenation Using Anisotropic Pd–Au Nanorods Studied at the Single-Particle Level." Journal of the American Chemical Society 137.2 (2015): 948-957.

43. Zhang, Zhenyi, et al. "Selective photocatalytic decomposition of formic acid over AuPd nanoparticle-decorated TiO_2nanofibers toward high-yield hydrogen production." Applied Catalysis B: Environmental 162 (2015): 204-209.

44. Tsutsumi, Ken, Naoko Kashimura, and Kenji Tabata. "Photo-Assisted Hydrogen Evolution in Aqueous Solution of Formic Acid with Silicon which is supported with Noble Metals." Silicon 7.1 (2015): 43-48.

45. Yoneyama, Hiroshi, Nobuyuki Matsumoto, and Hideo Tamura. "Photocatalytic decomposition of formic acid on platinized n-type silicon powder in aqueous solution." Bulletin of the Chemical Society of Japan 59.10 (1986): 3302-3304.

46. Li, Yuexiang, et al. "Effects of electrolyte NaCl on photocatalytic hydrogen evolution in the presence of electron donors over Pt/TiO_2." Journal of Molecular Catalysis A: Chemical 341.1 (2011): 71-76.

47. Zhang, Xianghui, et al. "Photocatalytic hydrogen evolution with simultaneous degradation of organics over (CuIn) 0. 2 Zn 1. $6S_2$ solid solution."International Journal of Hydrogen Energy 38.36 (2013): 15985-15991.

48. Halasi, Gyula, Gábor Schubert, and Frigyes Solymosi. "Photolysis of HCOOH over Rh deposited on pure and N-modified TiO_2." Catalysis letters 142.2 (2012): 218-223.

49. Lanese, Valeriano, et al. "Hydrogen production by photoreforming of formic acid in aqueous copper/TiO_2 suspensions under UV-simulated solar radiation at room temperature." international journal of hydrogen energy38.23 (2013): 9644-9654.

50. Loges, Björn, et al. "Hydrogen generation: catalytic acceleration and control by light." Chemical Communications 28 (2009): 4185-4187.

51. Onishi, Masayoshi. "Decomposition of formic acid catalyzed by hydrido (phosphonite) cobalt (I) under photoirradiation." Journal of molecular catalysis 80.2 (1993): 145-149.

52. Zielinska, Beata, Magdalena Janus, and Ryszard Kalenczuk. "Preparation, characterization and photocatalytic activity of $Co_3O_4/LiNbO_3$ composite."Open Chemistry 11.6 (2013): 920-926.

53. Boddien, Albert, et al. "Iron-catalyzed hydrogen production from formic acid."Journal of the American Chemical Society 132.26 (2010): 8924-8934.

54. I. Willner, Z. Goren, J. Chem. Soc., Chem. Commun. 1986, 172-173.

55. Kambe, Shiro, et al. "Photocatalytic hydrogen production with Cd (S, Se) solid solution particles: Determining factors for the highly efficient photocatalyst." Chemical physics letters 109.1 (1984): 105-109.

56. Zhu, Y. S., et al. "Visible-light-driven hydrogen generation from formic acid over CdS photoanode." International Journal of Hydrogen Energy (2015).

57. Li, Yuexiang, et al. "Synthesis of CdS nanorods by an ethylenediamine assisted hydrothermal method for photocatalytic hydrogen evolution." The Journal of Physical Chemistry C 113.21 (2009): 9352-9358.

58. Li, Yuexiang, et al. "Phosphate-assisted hydrothermal synthesis of hexagonal CdS for efficient photocatalytic hydrogen evolution." CrystEngComm 14.20 (2012): 6974-6982.

59. Zhang, Yao Jun, and Li Zhang. "Photocatalytic degradation of formic acid with simultaneous production of hydrogen over Pt and Ru-loaded CdS/Al-HMS photocatalysts." Desalination 249.3 (2009): 1017-1021.

60. Zhang, Yao Jun, Li Zhang, and Sheng Li. "Synthesis of Al-substituted mesoporous silica coupled with CdS nanoparticles for photocatalytic generation of hydrogen." international journal of hydrogen energy 35.2 (2010): 438-444.

61. Wang, Xi, Wen-chao Peng, and Xiao-yan Li. "Photocatalytic hydrogen generation with simultaneous organic degradation by composite CdS–ZnS nanoparticles under visible light." International Journal of Hydrogen Energy39.25 (2014): 13454-13461.

62. Yeh, H. M., et al. "Hydrogen production from formic acid solution by modified TiO_2 and titanate nanotubes in a two-step system under visible light irradiation." Water Science & Technology 69.8 (2014): 1676-1681.

63. Nedoluzhko, Aleksey I., Igor A. Shumilin, and Vitaly V. Nikandrov. "Coupled action of cadmium metal and hydrogenase in formate photodecomposition sensitized by CdS." The Journal of Physical Chemistry 100.44 (1996): 17544-17550.

64. Hu, Xun, and Gongxuan Lu. "Investigation of steam reforming of acetic acid to hydrogen over Ni–Co

65. Melius, C. F., N. E. Bergan, and J. E. Shepherd. "Effects of water on combustion kinetics at high pressure." Symposium (International) on Combustion. Vol. 23. No. 1. Elsevier, 1991.

66. Goddard, John D., Yukio Yamaguchi, and Henry F. Schaefer III. "The decarboxylation and dehydration reactions of monomeric formic acid." The Journal of chemical physics 96.2 (1992): 1158-1166.

67. Akiya, Naoko, and Phillip E. Savage. "Role of water in formic acid decomposition." AIChE Journal 44.2 (1998): 405-415.

68. Akiya, Naoko, and Phillip E. Savage. "Role of water in formic acid decomposition." AIChE Journal 44.2 (1998): 405-415.

69. Sasaki, Yasuyoshi, et al. "The effect of co-catalyst for Z-scheme photocatalysis systems with an Fe 3^+/Fe 2^+ electron mediator on overall water splitting under visible light irradiation." Journal of Catalysis 259.1 (2008): 133-137.

70. Dwivedi, Charu, et al. "An organic acid-induced synthesis and characterization of selenium nanoparticles." Journal of Nanotechnology 2011 (2011).

71. Gao, Feng, et al. "Synthesis of nanorods and nanowires using biomolecules under conventional-and microwave-hydrothermal conditions." Journal of Materials Science 43.7 (2008): 2377-2386..

72. Radad, Khaled, et al. "Recent advances in benefits and hazards of engineered nanoparticles." Environmental toxicology and pharmacology 34.3 (2012): 661-672.

73. Morose, Gregory. "The 5 principles of “design for safer nanotechnology”."Journal of cleaner production 18.3 (2010): 285-289.

74. Prasad, Kumar Suranjit, et al. "Biosynthesis of Se nanoparticles and its effect on UV-induced DNA damage." Colloids and Surfaces B: Biointerfaces 103 (2013): 261-266.

75. Triantis, T., et al. "Photocatalytic synthesis of Se nanoparticles using polyoxometalates." Catalysis Today 144.1 (2009): 2-6.

76. Karn, Barbara, Todd Kuiken, and Martha Otto. "Nanotechnology and in situ remediation: a review of the benefits and potential risks." Ciência & Saúde Coletiva 16.1 (2011): 165-178.

77. Ferreira, A. J., J. Cemlyn-Jones, and C. Robalo Cordeiro. "Nanoparticles, nanotechnology and pulmonary nanotoxicology." Revista Portuguesa de Pneumologia (English Edition) 19.1 (2013): 28-37.

78. Reijnders, Lucas. "Cleaner nanotechnology and hazard reduction of manufactured nanoparticles." Journal of Cleaner Production 14.2 (2006): 124-133.

79. Georgekutty, Reenamole, Michael K. Seery, and Suresh C. Pillai. "A highly efficient Ag-ZnO photocatalyst: synthesis, properties, and mechanism." The Journal of Physical Chemistry C 112.35 (2008): 13563-13570.

80. Xu, Hua, et al. "Size-dependent Mie's scattering effect on TiO_2 spheres for the superior photoactivity of H_2 evolution." The Journal of Physical Chemistry C 116.5 (2012): 3833-3839.

81. Fusi, M., et al. "Island organization of TiO_2 hierarchical nanostructures induced by surface wetting and drying." Langmuir 27.5 (2011): 1935-1941.

82. Aliwi, S. M., and KoF Al-Jubori. "Photoreduction of CO_2 by metal sulphide semiconductors in presence of H 2 S." Solar energy materials 18.3 (1989): 223-229.

83. Vogel, R., P. Hoyer, and H. Weller. "Quantum-sized PbS, CdS, Ag2S, Sb2S3, and Bi2S3 particles as sensitizers for various nanoporous wide-bandgap semiconductors." The Journal of Physical Chemistry 98.12 (1994): 3183-3188.

84. Candelaria, Stephanie L., et al. "Nanostructured carbon for energy storage and conversion." Nano Energy 1.2 (2012): 195-220.

85. Stroyuk, Alexander L., et al. "Photopolymerization of water-soluble acrylic monomers induced by colloidal CdS and Cd x Zn1− x S nanoparticles."Colloid and Polymer Science 286.5 (2008): 489-498.

86. Liu, Maochang, et al. "Manganese doped cadmium sulfide nanocrystal for hydrogen production from water under visible light." international journal of hydrogen energy 37.1 (2012): 730-736.

87. Zeng, Ting, et al. "Effective Electrochemistry of Human Sulfite Oxidase Immobilized on Quantum-Dots-Modified Indium Tin Oxide Electrode." ACS Applied Materials & Interfaces 7.38 (2015): 21487-21494.

88. Chen, Zhang, and Yi-Jun Xu. "Ultrathin TiO2 layer coated-CdS spheres core–shell nanocomposite with enhanced visible-light photoactivity." ACS applied materials & interfaces 5.24 (2013): 13353-13363.

89. Geelhoed, Jeanine S., Tjisse Hiemstra, and Willem H. Van Riemsdijk. "Phosphate and sulfate adsorption on goethite: single anion and competitive adsorption." Geochimica et cosmochimica acta 61.12 (1997): 2389-2396.

90. Nowack, Bernd, and Thomas D. Bucheli. "Occurrence, behavior and effects of nanoparticles in the environment." Environmental pollution 150.1 (2007): 5-22.

91. Cupaioli, Francesca A., et al. "Engineered nanoparticles. How brain friendly is this new guest?." Progress in neurobiology 119 (2014): 20-38.

92. Xu, Bing, Ren Guo Song, and Chao Wang. "Preparation and characterization of Ag, Au and Ti metal nanoparticles colloids by pulsed laser ablation in liquids." Advanced Materials Research. Vol. 415. 2012.

93. Radad, Khaled, et al. "Recent advances in benefits and hazards of engineered nanoparticles." Environmental toxicology and pharmacology 34.3 (2012): 661-672.

94. Ju-Nam, Yon, and Jamie R. Lead. "Manufactured nanoparticles: an overview of their chemistry, interactions and potential environmental implications."Science of the total environment 400.1 (2008): 396-414.

95. Meyers, Marc A., A. Mishra, and David J. Benson. "Mechanical properties of nanocrystalline materials." Progress in Materials Science 51.4 (2006): 427-556.

96. Shirsat, Shubhangi, et al. "Selenium nanostructures: microbial synthesis and applications." RSC Advances 5.112 (2015): 92799-92811.

97. Letchford, Kevin, and Helen Burt. "A review of the formation and classification of amphiphilic block copolymer nanoparticulate structures: micelles, nanospheres,

nanocapsules and polymersomes." European journal of pharmaceutics and biopharmaceutics 65.3 (2007): 259-269.

98. Ranjit, K., and A. A. Baque. "Nanoparticle: An overview of preparation, characterization and application." Int. Res. J. Pharm 4.4 (2013): 47-57.

99. Kango, Sarita, et al. "Surface modification of inorganic nanoparticles for development of organic–inorganic nanocomposites—A review." Progress in Polymer Science 38.8 (2013): 1232-1261.

100. Mittal, Amit Kumar, Yusuf Chisti, and Uttam Chand Banerjee. "Synthesis of metallic nanoparticles using plant extracts." Biotechnology advances 31.2 (2013): 346-356

101. Thakkar, Kaushik N., Snehit S. Mhatre, and Rasesh Y. Parikh. "Biological synthesis of metallic nanoparticles." Nanomedicine: Nanotechnology, Biology and Medicine 6.2 (2010): 257-262.

102. Virk, Hardev Singh. "Synthesis and Characterization of Metal and Semiconductor Nanowires." Solid State Phenomena. Vol. 201. 2013.

103. Mo, D., et al. "Preparation and characterization of CdS nanotubes and nanowires by electrochemical synthesis in ion-track templates." Journal of Crystal Growth 310.3 (2008): 612-616.

104. Dongre, J. K., Vikas Nogriya, and M. Ramrakhiani. "Structural, optical and photoelectrochemical characterization of CdS nanowire synthesized by chemical bath deposition and wet chemical etching." Applied Surface Science 255.12 (2009): 6115-6120.

105. Jang, Jum Suk, Upendra A. Joshi, and Jae Sung Lee. "Solvothermal synthesis of CdS nanowires for photocatalytic hydrogen and electricity production." The Journal of Physical Chemistry C 111.35 (2007): 13280-13287.

106. Dongre, J. K., Vikas Nogriya, and M. Ramrakhiani. "Structural, optical and photoelectrochemical characterization of CdS nanowire synthesized by chemical bath deposition and wet chemical etching." Applied Surface Science 255.12 (2009):6115-6120.

107. Garadkar, K. M., et al. "Characterization of CdS thin films synthesized by SILAR method at room temperature." Arch. Appl. Sci. Res 2 (2010): 429-437.

108. S. Kar, S. Chaudhuri J. Phys. Chem. B, 110 (2006), pp. 4542–454

109. Dongre, J. K., Vikas Nogriya, and M. Ramrakhiani. "Structural, optical and photoelectrochemical characterization of CdS nanowire synthesized by chemical bath deposition and wet chemical etching." Applied Surface Science 255.12 (2009): 6115-6120.

110. Dongre, J. K., Vikas Nogriya, and M. Ramrakhiani. "Structural, optical and photoelectrochemical characterization of CdS nanowire synthesized by chemical l bath deposition and wet chemical etching." Applied Surface Science 255.12 (2009): 6115-6120.

111. Mathew, Ammu, P. R. Sajanlal, and Thalappil Pradeep. "Selective Visua Detection of TNT at the Sub-Zeptomole Level." Angewandte Chemie International Edition 51.38 (2012): 9596-9600.

112. Kim, Seon Ho, et al. "Low temperature synthesis and growth mechanism of Ag nanowires." Journal of Alloys and Compounds 433.1 (2007): 261-264.

113. Kim, Seon Ho, et al. "Low temperature synthesis and growth mechanism of Ag nanowires." Journal of Alloys and Compounds 433.1 (2007): 261-264.

114. Dongre, J. K., Vikas Nogriya, and M. Ramrakhiani. "Structural, optical and photoelectrochemical characterization of CdS nanowire synthesized by chemical bath deposition and wet chemical etching." Applied Surface Science 255.12 (2009): 6115-6120.

115. Chu, Yuan-Chih, Cheng-Chien Wang, and Chuh-Yung Chen. "Synthesis of luminescent and rodlike CdS nanocrystals dispersed in polymer templates."Nanotechnology 16.1 (2005): 58.

116. Mulvaney, P., et al. "Silica encapsulation of quantum dots and metal clusters." Journal of Materials Chemistry 10.6 (2000): 1259-1270.

117. Correa-Duarte, Miguel A., Michael Giersig, and Luis M. Liz-Marzan. "Stabilization of CdS semiconductor nanoparticles against photodegradation by a silica coating procedure." Chemical Physics Letters 286.5 (1998): 497-501.

118. Bruchez, Marcel, et al. "Semiconductor nanocrystals as fluorescent biological labels." science 281.5385 (1998): 2013-2016.

119. Qi, Limin, Helmut Cölfen, and Markus Antonietti. "Synthesis and characterization of CdS nanoparticles stabilized by double-hydrophilic block copolymers." Nano Letters 1.2 (2001): 61-65.

120. Hirai, Takayuki, Tsuyoshi Saito, and Isao Komasawa. "Stabilization of CdS nanoparticles immobilized on thiol-modified polystyrene particles by encapsulation with polythiourethane." The Journal of Physical Chemistry B105.40 (2001): 9711-9714.

121. Zhang, Jun, et al. "Size control and photoluminescence enhancement of CdS nanoparticles prepared via reverse micelle method." Solid State Communications 124.1 (2002): 45-48.

122. Li, Yunchao, et al. "Controlled synthesis of CdS nanorods and hexagonal nanocrystals." Journal of Materials Chemistry 13.10 (2003): 2641-2648.

123. Qi, Limin, Helmut Cölfen, and Markus Antonietti. "Synthesis and characterization of CdS nanoparticles stabilized by double-hydrophilic block copolymers." Nano Letters 1.2 (2001): 61-65.

124. Caponetti, E., et al. "Synthesis, size control, and passivation of CdS nanoparticles in water/AOT/n-heptane microemulsions." Materials Science and Engineering: C 23.4 (2003): 531-539.

125. Wang, Xiuli, et al. "Shape-Controlled Synthesis of CdS Nanostructures via a solvothermal method." Crystal Growth & Design 10.12 (2010): 5312-53

Chapter 2

Experimental

2.1. Chemicals Used

All chemicals were of high purity grade and used without further purification. $Cd(NO_3)_2.4H_2O$, $Pb(NO_3)_2$, were purchased from Merck, NaOH from Fluka and Formic acid [(LR) grade (>90%)] was purchased from Sigma Aldrich.

All solvents were of analytical grade. Methanol was purchased from Dae Jung DCM, Acetone, Ethylenediamine, CS_2 and Octylamine were purchased from Sigma Aldrich.

2.2. Instrumentation

Melting point of the synthesized complex and ligand was determined in open capillary tube by using Sanyo electro thermal melting point apparatus. Shimadzu double beam Spectrophotometer 1800 was used to take the UV-Vis spectra of nanoparticles. UV analyze lamp SN: 500412 was used to provide UV source whose wavelength was adjusted at 250nm. In order to confirm the synthesis of cadmium sulphide nanoparticles, X-ray diffraction analysis was done. The analysis was performed at instrument PAN analytical X´Pert. The instrument has Cu Kά radiation wavelength 1.5418Å and values of 2 theta was maintained from 10 to 80. The NMR spectra were recorded on Bruker AC 300 MHz-FT-NMR spectrometer for ^{13}C and ^{1}H in various solvents like chloroform, acetone, and DMSO as solvent. Chemical shifts δ are given in ppm using DMSO as internal reference. Elemental analysis was carried out on the JED-2300/2300F Energy Dispersive X-ray Analyzer for determination of % composition of cadmium and sulpher atoms. Microscopic Studies were done on the JSM-6490LA, high-performance, Scanning Electron Microscope (SEM). The Infra-red absorption spectrum was recorded on a Bio-Rad Excalibur FTS model 3000MX in frequency range of 4000-400 cm^{-1}.

2.3. General Synthetic Method for ligand

Dithiocarbamtes ligands were synthesized by reported method[]. Synthesis of these ligands was carried out by reaction of secondary amine with NaOH followed by subsequent addition of CS_2 in the presence of methanol as a solvent at 0°C [1].

The presence of S as a donor atom makes these dithiocarbamate a viable ligand. Stoichiometric amount of secondary amine were dissolved in methanol and equivalent moles of NaOH was added to this reaction mixture. After complete dissolution of NaOH, equivalent amount of CS_2 was added drop wise keeping temperature around 0°C. The resulting solution was stirred for 8 hours and after that the solution was rotary evaporated to get corresponding salts of dithiocarbamate ligand.

2.3.1 Structure of Dithiocarbamate

The structure of monoanionic dithio ligands [10] can be represented by four different resonance structures shown in **Figure 2.1.**

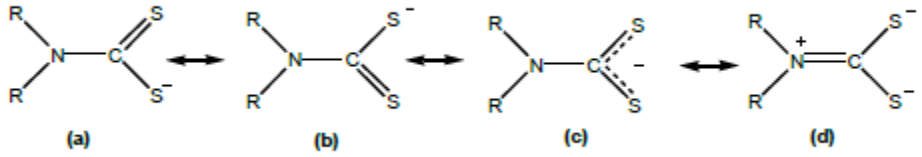

Figure 2.1 Canonical forms of the dithiocarbamate ligand

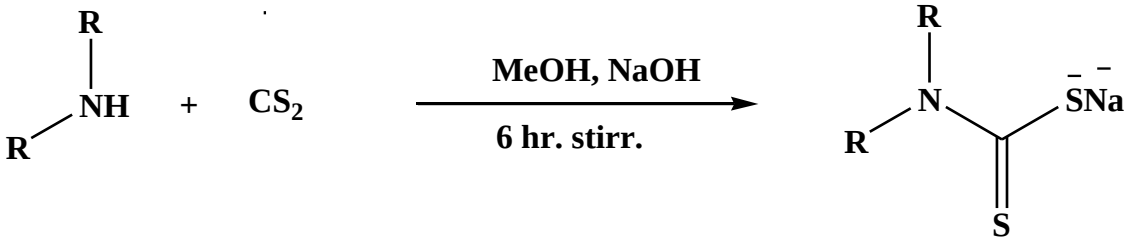

General scheme for ligand synthesis

R groups are

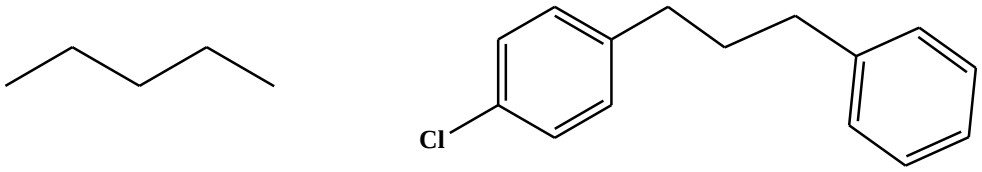

1) **2)**

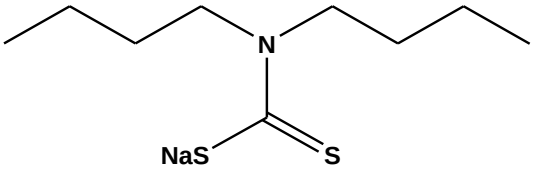

sodium dibutylcarbamodithioate

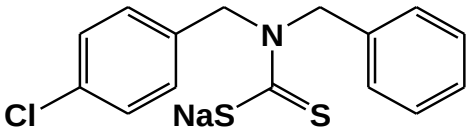

sodium 4-chlorobenzyl(benzyl)carbamodithioate

Figure 2.2 Structure of ligand L_1 and L_2

2.4. Synthetic Procedure for Cadmium(II)Dithiocarbamate Complexes:

$Cd(NO_3)_2.4H_2O$ was dissolved in methanol and added to the methanolic dithiocarbamate salt solution drop wise by dropping funnel. This mixture was maintained at stirring for 3 hours. After the completion of reaction, mixture was filtered and residue was washed three time with distilled water and then methanol.

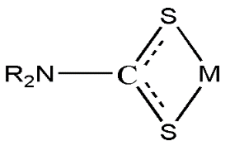

Isobidentate

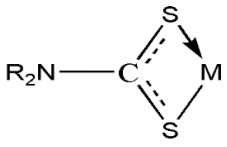

Anisobidentate

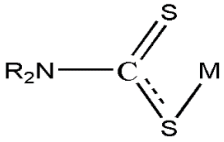

Monodentate

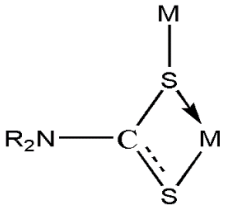

Triconnective

Figure 2.3 Coordination modes of dithiocarbamate ligand

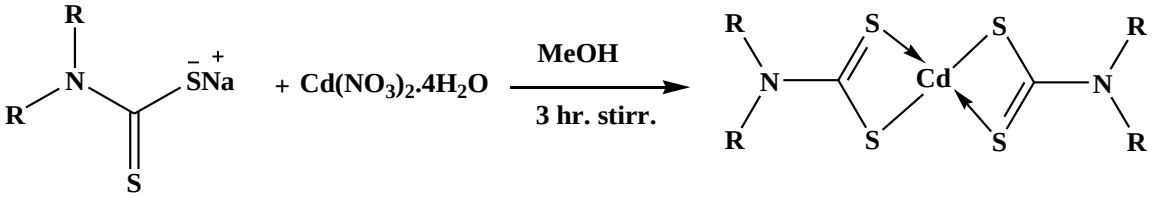

General scheme for complex synthesis

Complex R_1

Synthesis of complex R_1 was carried out by reacting 0.004moles (1g) of ligand $C_9H_{18}NS_2Na$ (Sodium dibutylcarbamodithioate) with 0.616g of $Cd(NO_3)_2.4H_2O$ salt solution with ligand to metal molar ratio 2 : 1 respectively at room temperature. The obtained product was washed with distilled water and methanol.

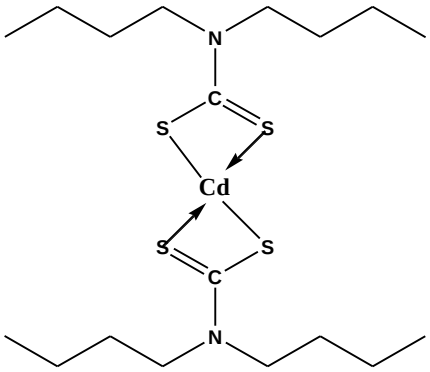

Figure 2.4 Cd(II) dibutylcarbamodithioate complex R_1

Complex R_2

Complex R_2 was synthesized by the reaction of 0.0035 moles (1g) of ligand $C_{15}H_{12}NS_2$ (Sodium 4-chlorobenzyl(benzyl)carbamodithioate) with 0.55g of $Cd(NO_3)_2.4H_2O$ salt solution. Stoichiometric amount of ligand was dissolved in methanol and allowed to react with Cd salt solution with a ligand to metal molar ratio 2: 1 in a two neck flask. The reaction mixture was maintained for three hours stirring at room temperature. The product obtained in good yield was then filtered and washed with distilled water and methanol.

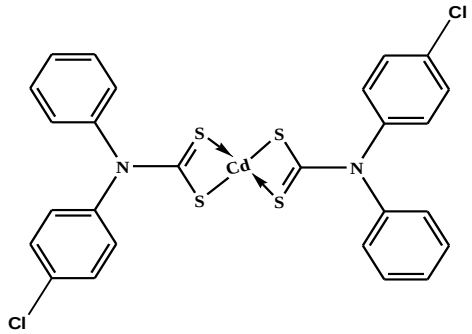

Figure 2.5 Cd(II) Sodium 4-chlorobenzyl(benzyl)carbamodithioate complex R_2

2.5. General Synthetic Scheme for CdS Nanoparticles

Decomposition of synthesized complex was carried out in two neck flask by addition of 10mL ethylenediamine or octylamine as a decomposing solvent. Reaction set up was maintained at constant stirring, smoothly and constantly rising the heating up to decomposition temperature. The temperature of reaction media was allowed to rise up to 120° C, yellow color CdS nanoparticles were obtained which were dispersed in methanol and then filtered. The product was washed with methanol and dried in oven at $70C^0$. H_2S was released during decomposition which was allowed to pass by side tube through $Pb(NO_3)_2$ aqueous solution and form PbS, as indication of the completion of reaction.

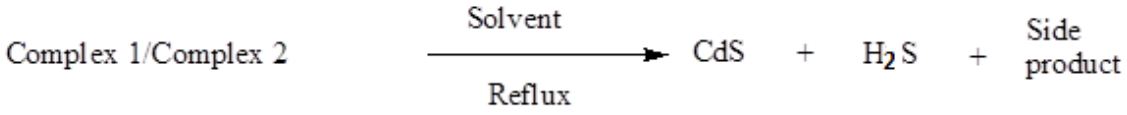

General scheme for CdS nanoparticle synthesis

References

1. P. Bera, C.H. Kim, S.I. Seok, Inorg. Chim. Acta 362 (2009) 2603.
2. N. Pradhan, A. Pal, T. Pal, Catalytic reduction of aromatic nitro compounds by coinage metal nanoparticles, Langmuir 17 (2001) 1800–1802.
3. D.M. Dotzauer, J. Dai, L. Sun, M.L. Bruening, Catalyticmembranesprepared using adsorption of polyelectrolyte/metal nanoparticle films in porous supports, Nano Lett. 6 (2006) 2268–2272
4. N.M. Mahmoodi, M. Arami, N.Y. Limaee, N.S. Tabrizi, Decolorization and aromaticring degradation kinetics of Direct Red 80 byUVoxidation in the presence of hydrogen peroxide utilizing TiO_2 as a photocatalyst, Chem. Eng. J. 112 (2005) 191–196.
5. I.K. Konstantinou, T.A. Albanis, TiO_2-assisted photocatalytic degradation of azo dyes in aqueous solution: kinetic and mechanistic investigations: a review, Appl. Catal. B: Environ. 49 (2004) 1–14
6. J. Wang, R.H. Li, Z.H. Zhang, W. Sun, R. Xu, Y.P. Xie, Z.Q. Xing, X.D. Zhang, Efficient photocatalytic degradation of organic dyes over titanium dioxide coating upconversion luminescence agent under visible and sunlight irradiation, Appl. Catal. A: Gen. 334 (2008) 227–233.
7. R.K. Wahi, W.W. Yu, Y. Liu, M.L. Mejia, J.C. Falkner, W. Nolte, V.L. Colvin, Photodegradation of Congo Red catalyzed by nanosized TiO2, J. Mol. Catal. A: Chem.242 (2005) 48–56.
8. S. Kaur, V. Singh, TiO2 mediated photocatalytic degradation studies of Reactive Red 198 by UV irradiation, J. Hazard. Mater. 141 (2007) 230–236.
9. K. D. Karlin, *Prog. Inorg. Chem*., John Wiley and Sons, Inc. New Jersey, **2005**, 5

CHAPTER 3

3.1 Physical data of ligand and complex

Physical data of the ligand L_1 and L_2 is given in **Table 3.1**. Ligand L_1 off white in colour while ligand L_2 is white in colour and soluble in Chloroform, DMSO and DMF. Physical data of the complexes is shown in **Table 3.2**, both complexes are of white colour and have solubility in DMSO, DCM and DMF.

Table 3.1 Physical data of Dithiocarbamate ligands L_1 and L_2

Sr.no.	Molecular formula	Physical state	Melting point	Solubility
1	$C_9H_{18}NS_2Na$	Off white solid	150 °C	DMSO, DMF,
2	$C_{15}H_{12}NS_2Na$	white solid	175 °C	DMSO, DCM,

Table 3.2 Physical data of R1 and R2 complexes

Sr no.	Molcular formula	Physical state	Melting point	Solubility
1	$CdC_{18}H_{36}N_2S_4$	White colour	280-285 °C	DCM,DMSO,DMF
2	$CdC_{30}H_{24}N_2S_4$	White colour	298-302 °C	DCM,DMSO,DMF

3.2. Structural Elucidation

For structural elucidation Nuclear Magnetic Resonance Spectroscopy was performed.

Nuclear Magnetic Resonance Spectroscopy

3.2.1 NMR studies of ligand L_2

^{1}H NMR $CDCl_3$-d6, 300MHz, δ(ppm):δ=4.05–3.99(t, 4H, N-CH_2), δ=1.78-1.68(m,4H,-CH_2), δ=1.40-1.38(m,4H,-CH_2), δ=1.33-1.28(t, 6H, -CH_3)

^{13}CNMR ($CDCl_3$-d6, 75MHz, δ(ppm): δ=53.69(-CH_2), δ(ppm): δ=28.77(-CH_2), δ(ppm): δ=19.89(-CH_2), δ(ppm): δ=13.01(-CH_2), δ(ppm): δ=209.95(C=S). The spectra are shown in **Figures 3.1 and 3. 3**

3.2.2 NMR studies of Complex R_2

^{1}H NMR $CDCl_3$-d6, 300MHz, δ(ppm):δ=3.76(t, 4H, N-CH_2), δ=1.68(m,4H,-CH_2), δ=1.27(m,4H,-CH_2), δ=0.90(t, 6H, -CH_3)

^{13}CNMR ($CDCl_3$-d6, 75MHz, δ(ppm): δ=55.86(-CH_2), δ(ppm): δ=29.05(-CH_2), δ(ppm): δ=20.03(-CH_2), δ(ppm): δ=14.14(-CH_2), δ(ppm): δ=204.35(C=S) . The spectra are shown in **Figure 3.2 and 3.4**

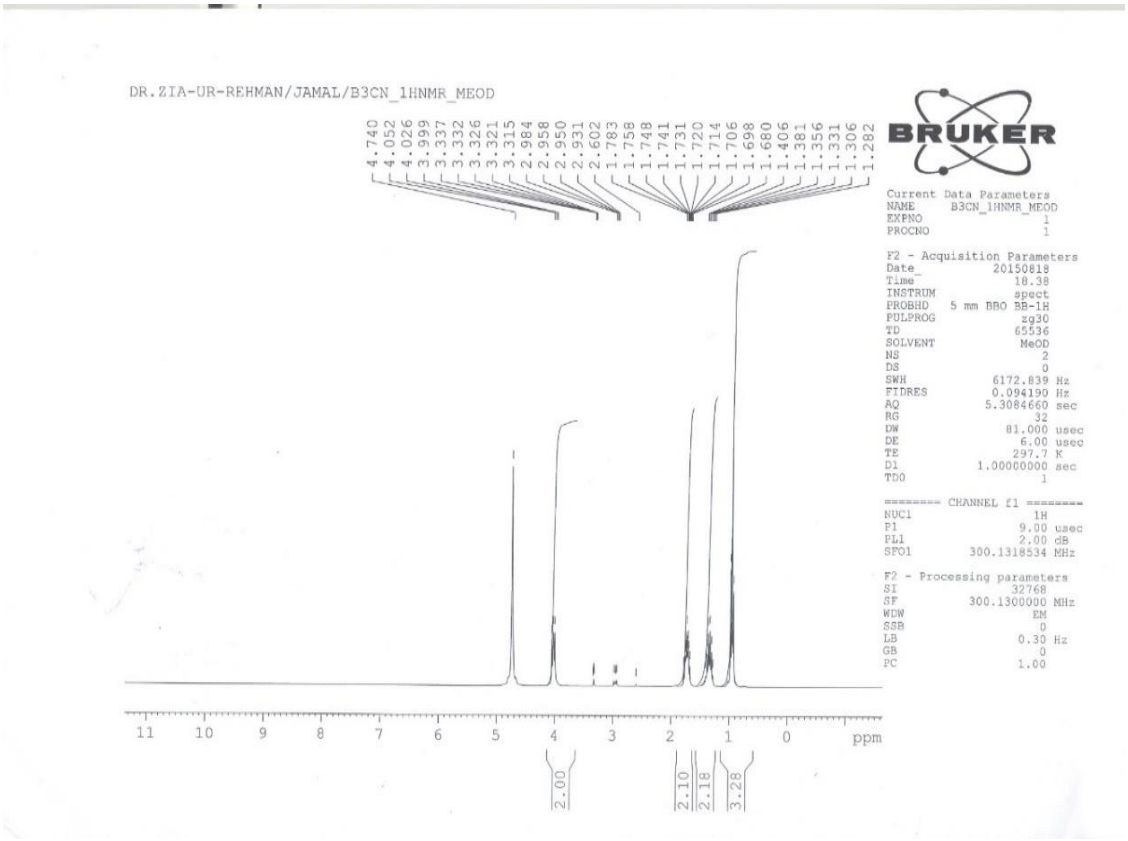

Figure 3.1 ^{1}H NMR of L_1

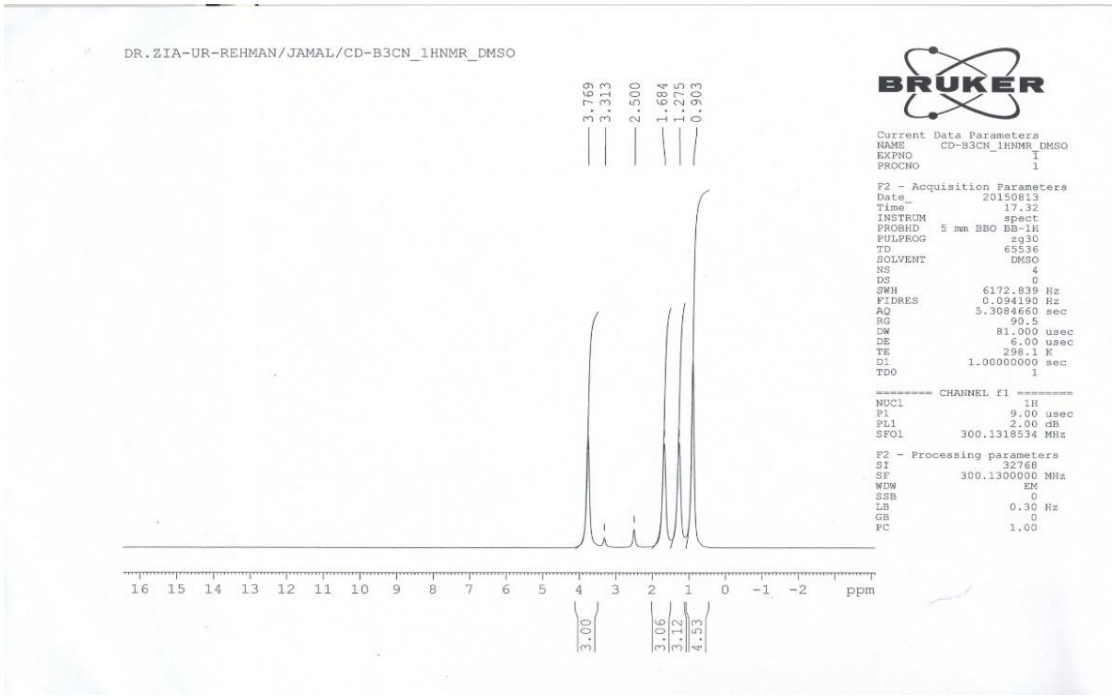

Figure 3.2 ^{1}H NMR spectrum of R1

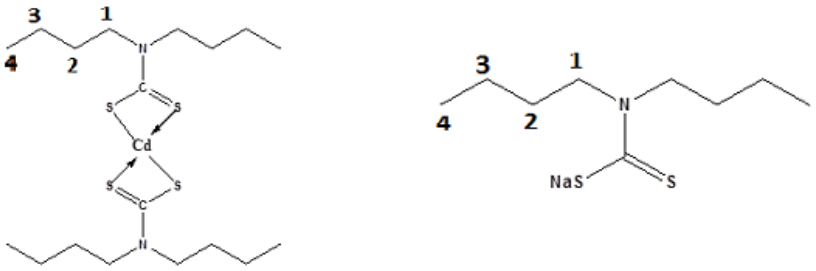

Table 3.3 ^{1}H NMR data for ligand (L1) and its complex (R1)

Hydrogen	1(ppm)	2	3	4
Ligand (L_1)	4.03	1.73	1.34	1.28
Complex (R_1)	3.76	1.68	1.27	0.90

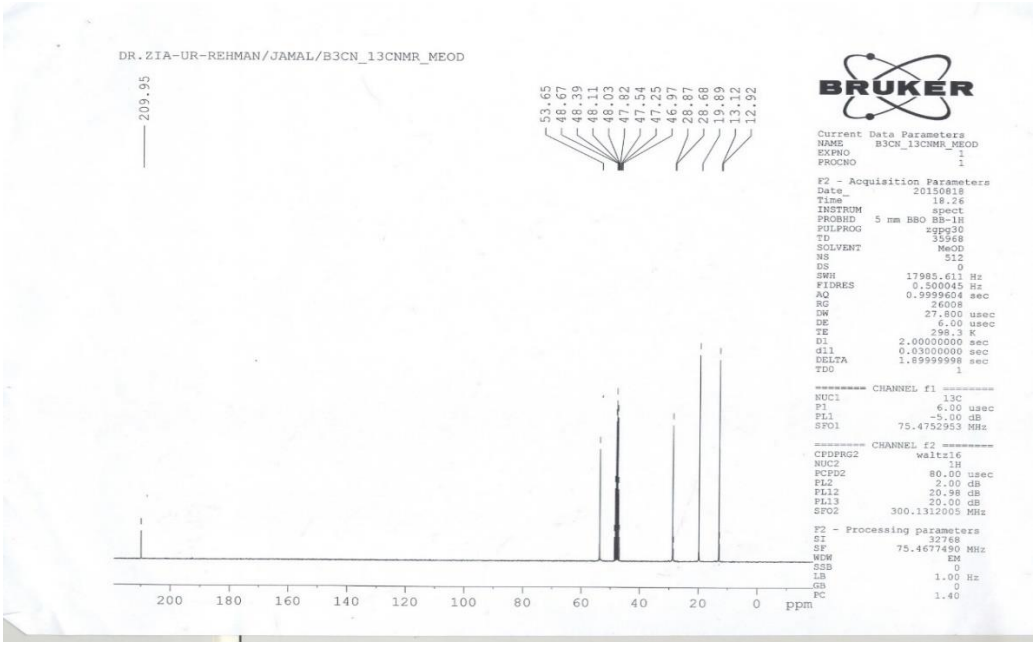

Figure 3.3 ^{13}C NMR spectrum of L_1

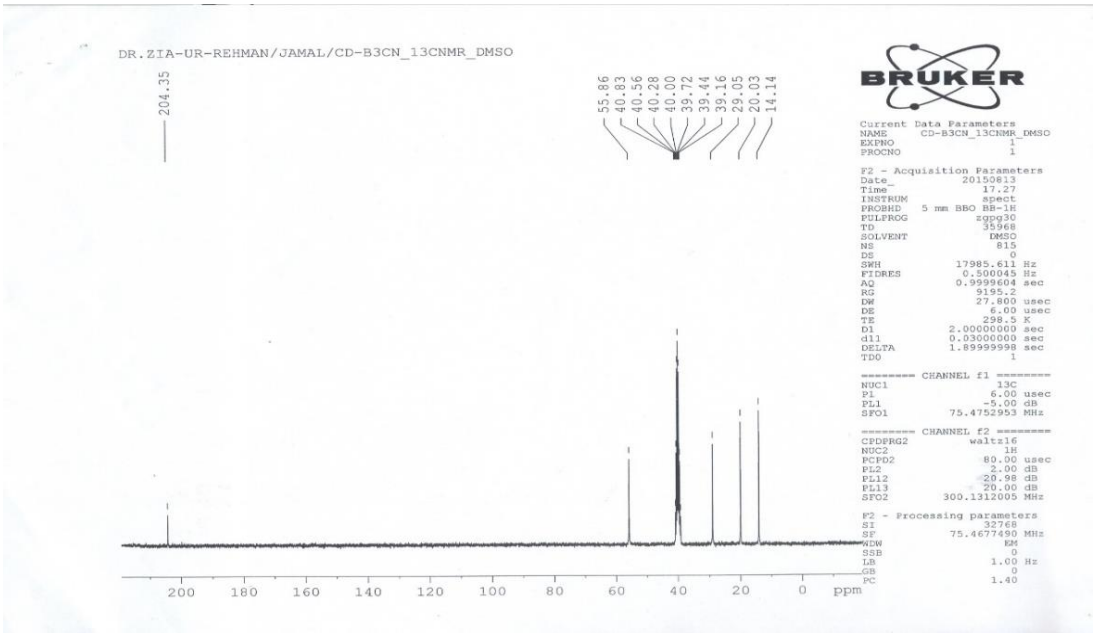

Figure 3.4 ^{13}C NMR spectrum of R_1

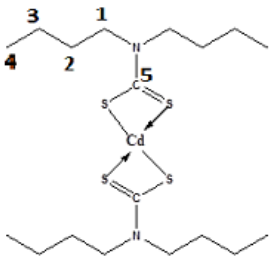

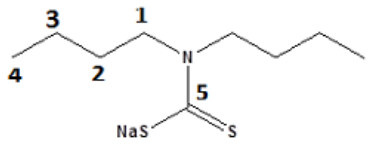

Table 3.4 ^{13}C NMR data for Ligand (L_1) and complex (R_1)

Carbon	1(ppm)	2	3	4	5
Ligand(L_1)	53.7	28.8	19.9	13.0	209.9
Complex(R_1)	55.9	29.1	20.01	14.1	204.4

3.3. Elemental and FTIR Analysis

The elemental analyses and determination of of synthesized CdS NPs were carried out by Fourier Transform Infrared Spectroscopy (FTIR) Spectroscopy and Energy Dispersive X-ray Spectroscopy (EDS).

3.3.1 Fourier Transform Infrared (FTIR) Spectroscopy

The most important bands recorded in the FT-IR spectra of the synthesized cadmium sulphide nanoparticle are listed in **Table 3.5**. Tentative assignments are made according to the literature [11, 12]. FTIR is used to study the stretching vibrations of the synthesized nanoparticles. It is used to determine the functional groups and types of bonds present in the sample. The dried CdS nanoparticles mixed with KBr were characterized with FTIR. **Table 3.5** contains the explanation of the peaks obtained by the synthesized CdS nanoparticles [1]. The absorption peaks in the range of 3380-3450 cm^{-1} could be attributed to the NH_2 group of ethylenediamine adsorbed on the CdS nanoparticles. The two bands at 2881 cm^{-1} and 2763 cm^{-1} were assigned to C-H stretching vibration. Sharp peak at 1612 cm^{-1} indicates NH_2 bending. Peak at 1410 attributed to C=S asymmetric stretching of thiourea. Small peak near 400-470cm^{-1} may be indicated the formation of CdS nanoparticles as this region was assigned to metal-sulphur (M-S) bond [1, 2].

Table 3.5 IR Stretching Vibrations of CdS Nanoparticles

Peak	Region(cm^{-2})	Intensity	Significance
1	400-470	Small peak	Cd-S
2	820-860	Sharp	S-S-S bending
3	1410	Sharp	C=S asymmetric stretching
4	1612	Medium	NH_2 bending
5	2700 up to 2900	Sharp	C-H stretching vibration,
6	3380 and 3450	Medium	NH_2 Stretching vibration, two bands

3.3.2. Energy Dispersive X-ray Spectroscopy (EDS)

Figure 3.5 reveals the EDS spectra of the synthesized CdS NP (CdS-1, CdS-3), the presence of Cd and S peaks confirmed the formation of pure CdS and no other elemental impurity. The average atomic percentage ratio of Cd:S 43.80:56.20 for CdS-1, 54.0:46.0 for CdS-2. Other peaks in this figure of CdS-2 corresponded to aluminum, oxygen and magnesium, were because of sputter coating of glass substrate on the EDS stage and were not take in consideration of elemental analysis of Cd and S.

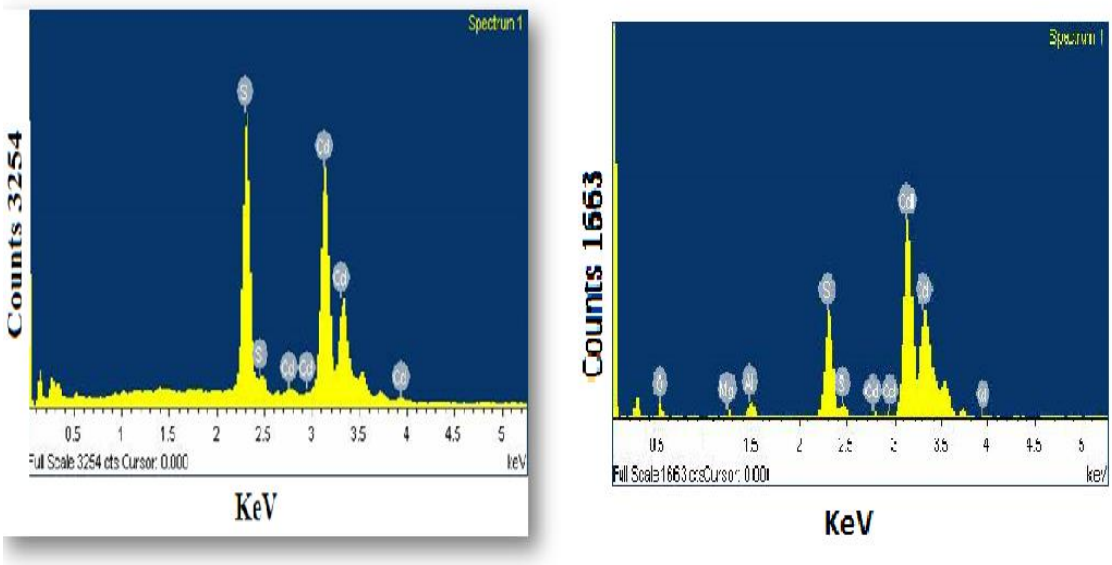

Figure 3.5. The EDS spectra of synthesized CdS nanoparticles (CdS-1, CdS-3)

3.4. Structural Analysis

The structural and morphological properties of the synthesized complexes and corresponding NPs were carried out by diffraction studies (using X-Ray Diffraction (XRD) Spectroscopy) and microscopic studies using Scanning Electron Microscopy (SEM) for NPs and Multinuclear Magnetic Resonance Spectroscopy (NMR) for complexes and their ligands.

3.4.1. Diffraction Studies

The Diffraction Studies were determined by using X-Ray Diffraction (XRD) Spectrometer.

Powder XRD of nano particles was done in order to find the phase purity and crystallite size of the nano particles. The crystallite size was calculated using Debye Scherer formula.

$$D = k\lambda/\beta cos\theta \qquad 3.1$$

K is the Scherer constant whose value is equal to 0.9

λ is the X-ray wavelength. Its value is 1.54 angstrom

β is the line broadening at half the maximum intensity (FWHM)

θ is the Bragg's angle

The XRD data shown below confirm the formation of hexagonal-wurtzite type and cubic-zinc blend type structured of CdS NP (CdS-1, CdS-2, CdS-3, CdS-4) synthesized via two different scheme. The XRD pattern displayed in **Figure 3.6** (CdS-1, CdS-2) shows that both NPs belongs to hexagonal-wurtzite type. The XRD pattern for CdS NP CdS-1 (**Figure 3.6**) can be consistently indexed on the basis of the hexagonal, W-type structure [3,4,5] in which the ten prominent lines correspond to the reflections at 2θ=25.0438° (100), 26.685° (002), 28.3095° (101), 36.8303° (102), 43.949^0 (110), 48.173° (103) and 52.110° (112).The weak 58.406^0 (202), 67.01^0 (203), 75.671^0 (105) were also observed. The peaks at 2θ=36.8303° and 48.173° are characteristic for hexagonal W-type structure [6, 7, 8]. Similarly the XRD spectrum from CdS-2 **(Figure 3.6)** exhibited peaks at 2θ=25.161°

(100), 26.856° (002), 28.619° (101), 36.985° (102), 44.036^0 (110), 48.232° (103) and 52.054° (112).The weak 58.536^0 (202), 67.104^0 (203), 75.985^0 (105) were also observed corresponding to hexagonal, W-type structure. The XRD spectrum from CdS-3 and CdS-4 **(Figure 3.7)** apparently exhibited only three broad peaks, centered at 2θ =26.79°, 44.01° and 52.09°. The main broad peak at 26.79° on close observation was found to be an overlap of multiple peaks, comprising of shoulders on both the sides at 2θ=24° and 28°, respectively, resulting from the overlap of (100), (002) and (101) peaks of hexagonal W-type structure. The increase in overlap in CdS-3 and CdS-4 **(Figure 3.7)** was obviously as a result of line broadening due to the smaller particle size in these samples as compared to CdS-1 and CdS-2 **(Figure 3.6).** However, the three most prominent peaks for cubic CdS with Z-type structure also occur at 26.79° (111), 44.01° (220) and 52.09° (311). Thus, the existence of cubic CdS could not be ruled out based on XRD information. Consequently, it can be decided that CdS-3 and CdS-4 **(Figure 3.7)** revealed prominent features of both phases and had a distorted structure resulting due to the fractional contents of both the phases [9, 10].

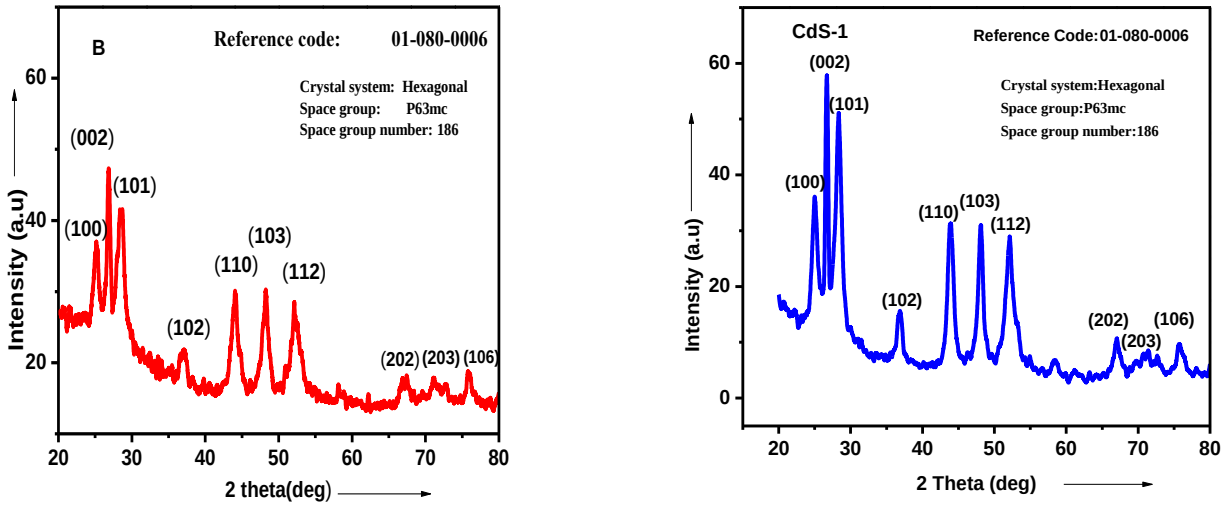

CdS-1 **CdS-2**

Figure 3.6 XRD pattern of nanoparticles synthesized via Ethylenediamine

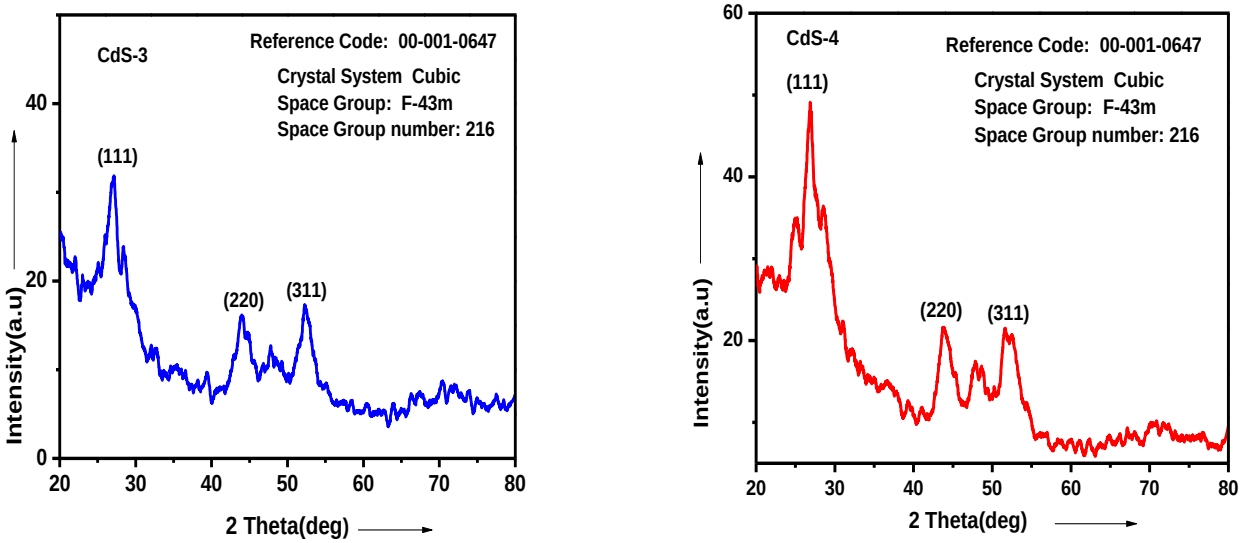

CdS-4 **CdS-3**

Figure 3.7 XRD pattern of nanoparticles synthesized via octylamine

Table 3.6 Crystallite size of nanoparticles obtained by Debye Sherer formula

CdS Nanoparticles	Crystalline phase	FWHM(in degree)	Crystallite size (nm)
CdS-1	Hexagonal	0.94	8.2
CdS-2	Hexagonal	0.47	11
CdS-3	Cubic + hexagonal	1.16	4
CdS-4	Cubic + hexagonal	1.15	6

The estimated X-ray size for CdS-2 (based on the FWHM) of the (101) peak was ~11nm.

3.5. Microscopic Studies

Microscopic Studies were done using Scanning Electron Microscope (SEM).

3.5.1. Scanning Electron Microscopy (SEM)

The SEM micrographs showed uniform size with very fine particle structure. **Figure 3.8** displays the SEM images of the synthesized CdS NP at 50000 times magnification (50kx).

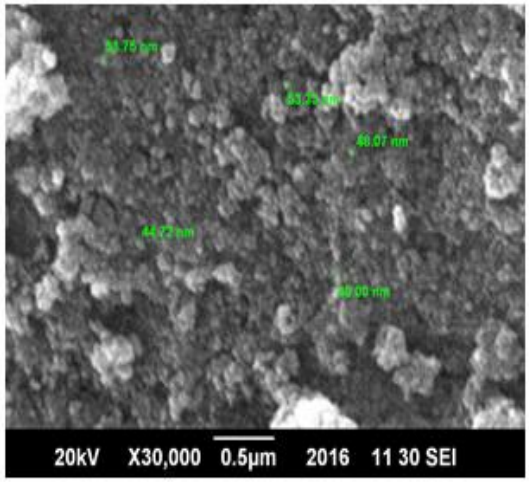

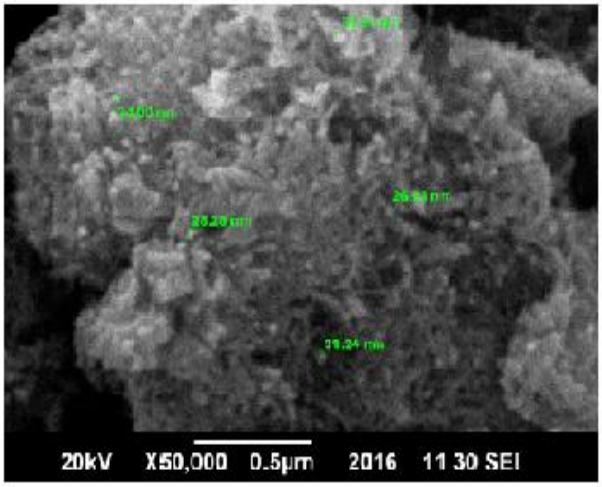

(CdS-1) Average size 47.97 nm **(CdS-3) Average size 29.5 nm**

Figure 3.8 SEM images of the CdS nanoparticles at 5000x magnification

3.6. Optical Analysis

3.6.1 UV-Visible (UV-Vis.) Spectroscopy

The UV-vis. spectroscopy gave the absorption spectra of the nanomaterials in the range of 200 to 800nm of solar spectrum. The absorption edge in bulk CdS is found almost at 515nm while in synthesized CdS nanoparticles the absorption edges were observed at lower wavelength indicated the smaller size of nanoparticles. Variation in band gap energy and absorption spectra was observed in these four types CdS nanoparticles. This variation is directly related and depends on reaction conditions, decomposing solvent and structure of precursor. In **Figure 3.9** particles CdS-1 and CdS-2 were synthesized from R_1 and R_2 **(Figure 2.4, 2.5)** complexes using ethylenediamine as a decomposing solvent, but in **(Figure 3.10)** for synthesis of particles CdS-3 and CdS-4, octylamine was used as a decomposing solvent. As ethylenediamine is a bidentate ligand and has chelating effect,

so coordinated to dithiocarbamate complexes more strongly as compared to monodentate like octylamine. Thus decomposition in case of ethylenediamine was difficult as compared to octylamine. The chances of smaller and spherical size particles increases in case of using monodentate decomposing solvent. From XRD both particles synthesized via scheme 2 **(Figure 3.10)** have cubic geometry with some mixed planes of hexagonal phase type .Shoulder appears on the right and left of (111) planes **(Figure 3.7)**.

Based on Tauc plot relation [13, 14] (**Figure 3.9, 3.10)** shows the plot of **$(\alpha.E)^2$** versus **eV** whose intercept on energy axis gave the band gap energy **(eV)** of the synthesized CdS (CdS-1, CdS-2, CdS-3, CdS-4) nanoparticles.

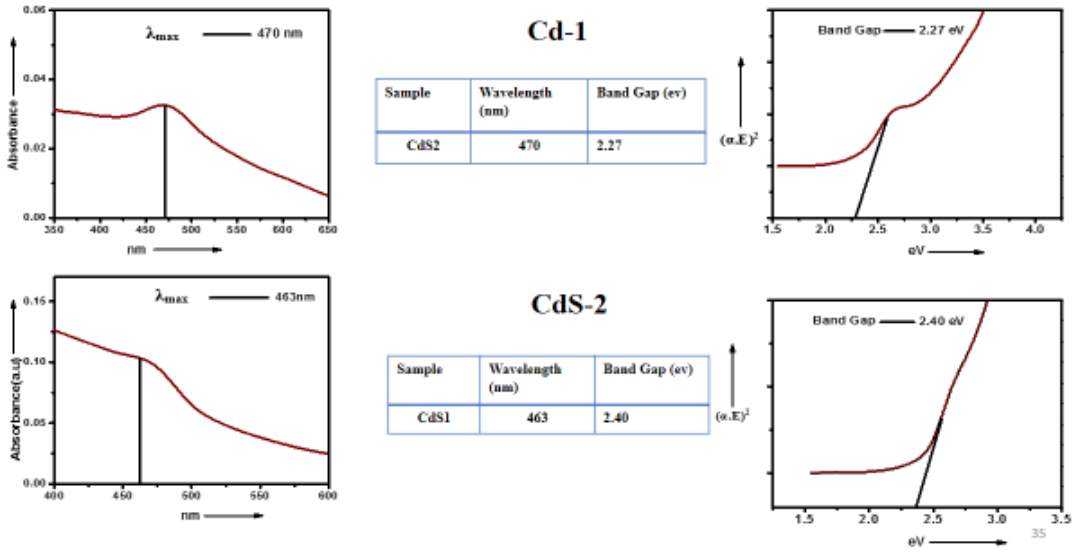

Figure 3.9 UV-Visible Spectra for CdS nanoparticles (CdS-1 and CdS-2) Synthesize via scheme 1

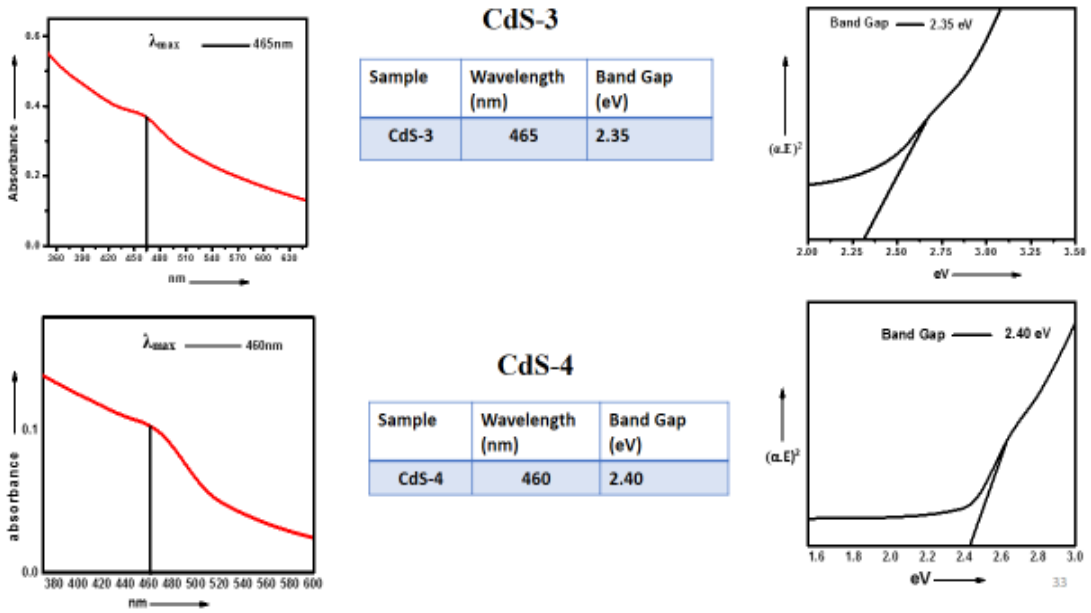

Figure 3.10 UV-Visible Spectra of CdS Nanoparticles (CdS-3 and CdS-4) Synthesizes via Scheme 2

3.7. Photocatalytic activity

The photocatalytic activity of the synthesized CdS nanoparticles was studied for photocatalytic decomposition of formic acid under visible light. The blank experiments were also separately carried out to check the dependence of the photocatalyst and co-catalyst on photocatalytic activity. Without addition of the photocatalyst and in presence of the photocatalyst under dark condition, no photocatalytic activity was recorded. Absence of co-catalyst did not show any appreciable decomposition of formic acid (**Figure 3.16**). In order to attain the superior photocatalytic activities of CdS nanoparticles, suitable co-catalyst under optimized condition should be loaded onto the photocatalyst.

3.7.1. Photocatalytic reactions

For an illumination source, a Xenon lamp (750 W, 45 A,) was used with an adjustable intensity 20-100 $mWCm^{-2}$. The wavelength >420nm was chosen as it coincided with an excitonic absorption peak of CdS. The experiments were performed under Nitrogen atmosphere in a photoreactor having 3.15 cm^2 illumination area and a sample volume of 4.5 mL. H_2 production was determined with a Shimadzu GC2014 gas chromatography (GC) equipped with a thermal conductivity detector. For the evaluation of H_2 generation,

each time 1 mL of the sample was injected to the GC. Simple calculation was done according to the standard peak of H_2.The H_2 formation rate was calculated as the molar amount of hydrogen generated per hour of illumination rate and per gram of CdS nanoparticles.

3.7.2. Reagents

All chemicals were of high purity grade and used without further purification for photocatalysis. Formic acid [(LR) grade (>90%)] was purchased from Sigma Aldrich. HCOONa was synthesized in lab by reacting of Na_2CO_3 with Formic acid in a 1:2 molar ratio. 4.0 M sodium formate solutions and 1mM both $CoCl_2.6H_2O$, and $NiCl_2.6H_2O$ solutions were prepared in formic acid to give a total volume of 20 mL. All solvents were of analytical grade and distilled water was used in all photocatalysis experiments.

3.7.3. At varying catalyst concentration

The hydrogen production rate was steadily increases as photons are continuously shoot up into the semiconductor. Quantitatively, the number of photons on the radiated area of photoreactor containing dilute solution are less because maximum photons are pass through the empty gaps in solution having no photocatalyst. They may also reflected by the wall of photoreactor without being absorbed. Reverse phenomenon shown by these photons in case of concentrated solution of photocatalyst. Most of photons trapped on the radiated area are absorb and less are being reflected. Active sites for reaction of photoctalysis provided by photocatalyst increases. From 170µM to 260µM there is continuous increase in $mmolh^{-1}$ of H_2 production. At maximum 1mM of CdS 16.4 ±2.2 $mmolH_2h^{-1}$ (**Figure 3.11**) generated. The total amount of photons absorbed by the photocatalyst thus increases and rate of photocatalysis correspond to H_2 generation also enhances. However at certain point of maximum critical concentration of photocatalyst the injection of photons to surface area of catalyst decreases and recombination of electrons and holes increases ,thus production rate of hydrogen start to decrease [15].To obtain a good photocatalytic efficiency with minimum optimal amount of photocatalyst are being discussed in this article **(Supporting table 3.7).**

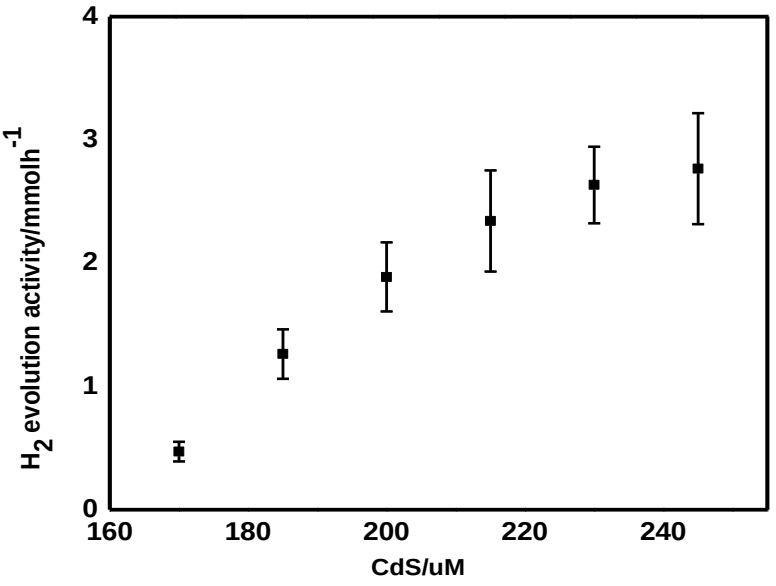

Figure 3.11 Photocatalytic H_2 generation using $CdS/CoCl_2$ at varying CdS concentration(160µM, 180µM, 200µM, 220µM, 240µM, and 260µM) [sunlight radiation; 1mM $CoCl_2$, 4.0M $NaHCO_2$ in 2.0 mL formic acid; activity was determined after 1 h irradiation]

3.7.4. At varying Sodium Formate concentration

The sodium formate solution has a high concentration of sodium ions and formate ions. The pH is above 7 and depends upon the concentration of sodium formate and the pK_a of formic acid, now the addition of formate to this mixture.

$$HCHO_2 + H_2O \rightleftharpoons H^+ + CHO^{2-} \qquad 3.2)$$

$$NaCHO_2 \longrightarrow Na^+ + CHO^{2-} \qquad 3.3)$$

The sodium formate solution adds sodium ions and formate ions which disturbs the formic acid equilibrium and driving it towards the reactants side. Because of this there, removes some hydronium ion from solution, and increasing the pH. Addition of the common ion (formate) to the formic acid equilibrium, result in increasing the pH of the mixture. During FA decomposition an intermediate product, formate, [16, 17], is almost added for promoting activity of catalyst [18, 19, 20, 21, 22]. It is reported that sodium formate (SF, $NaHCO_2$) can also liberate H_2 through a hydrolysis reaction with some homogenous catalysts.

$$HCO_2Na + H_2O\ (l) \rightarrow H_2\ (g) + NaHCO_3 \qquad 3.4)$$

Efficiency of H_2 generation can be further improved if SF could also generate H_2 in a heterogeneous photocatalysis. Moreover, SF in the reaction system plays important roles as not only the co-catalyst but also as a reducing agent and H_2 source with promising activity, selectivity, and stability for H_2 generation from both FA and SF in aqueous dispersed solution of CdS. At room temperature without CO contamination is of great interest to meet the demand of fuel cell applications on-broad [17] **(Figure 3.12, Supporting table 3.8).**

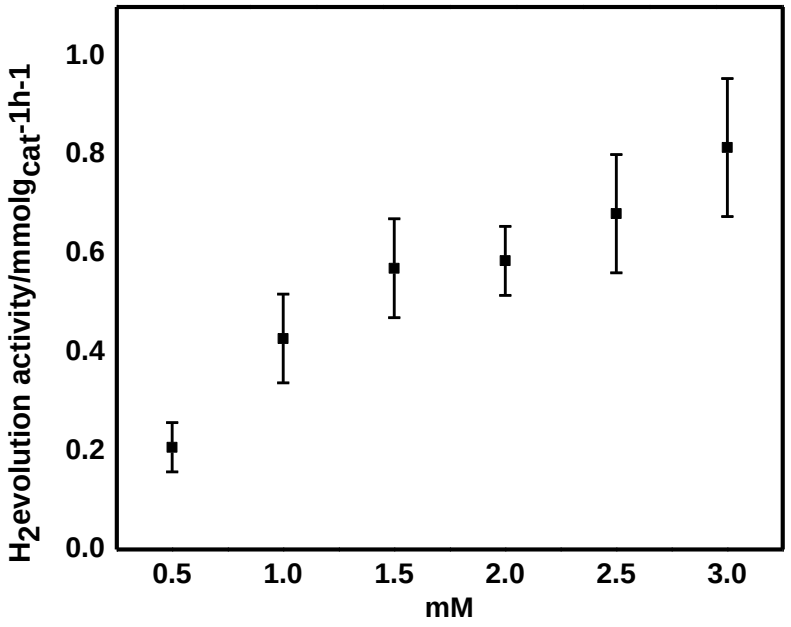

Figure 3.12 Photocatalytic decomposition of sodium formate (SF/FA) using CdS at varying sodium formate concentrations (0.5mM, 1.0mM, 1.5mM, 2.0mM, 2.5mM, and 3.0mM), [185µM CdS (24 µg mL^{-1}), 1mM $CoCl_2.6H_2O$ in 2.0 mL formic acid, pH not adjusted. Activity was determined after 1 h irradiation]

3.7.5 (a) At varying co-catalyst concentration

The photocatalytic activity of CdS photocatalyst without addition of co-catalyst ($CoCl_2.6H_2O$) was as low as 0.311 ±0.03 $mmolH_2\ h^{-1}g^{-1}$ and have very low life time

which is confirmed by the blue shift of UV visible spectrum, but was greatly enhanced after loading with $CoCl_2.6H_2O$ co-catalyst **(Figure 3.13)**. Similarly hydrogen production was gradually increased from 0.515 ±0.07 to 1.529 ±0.93 mmolH_2 $h^{-1}g^{-1}$ with turnover number maximum 437±10.0 at 1mM $CoCl_2.6H_2O$ loading. However, it was observed that, further loading from 1.5 to 2.5mM concentration of co-catalyst there is decrease in hydrogen production to minimum value of 0.414 ±0.18 mmolH_2 $h^{-1}g^{-1}$ with turnover number of 118 ±5.50 which is due to a shielding effect of the cobalt co-catalyst. After gradually loading of catalyst with co-catalyst, it was observed that catalyst surface area are covered by cobalt and become a shield in the path of trapping photons. These cobalt particles on the surface of photocatalyst drastically decreases luminescence intensity [23, 26, 27].Optimum amount of co-catalyst should be on the surface of CdS surface, by increasing concentration of co-catalyst to the optimum amount the surface barrier becomes higher and recombination of electron-hole pairs are efficiently suppressed by keeping them separate. On the other hand, further increasing the concentration of $CoCl_2.6H_2O$ charge region becomes very narrow and in turn facilitate the recombination of electron-hole pair. Increase in the doping amount enhances visible light absorption whereas it makes a recombination center between photogenerated carriers increase. Therefore, the volcano-type dependence was obtained [28]. Thus, samples beyond the optimum mass show poor photocatalytic activities [24]. There is homogeneous oxidation of FA by Co^{3+} ions [29]. The mechanism of FA-to-H_2 conversion could, therefore, comprise of formate oxidation by photogenerated holes and successive proton reduction by photoexcited electrons [31, 30]. The reductive half reaction, the oxidative half reaction, or both are enhanced by co-catalysts [26]. Co-catalysts on the surface of catalyst provide not only active site but also a shielding effect in the path of incident light. The photocatalytic activity, loading of the co-catalyst depends on keeping the balance between these two factors [25] **(Supporting table 3.9, 3.14).**

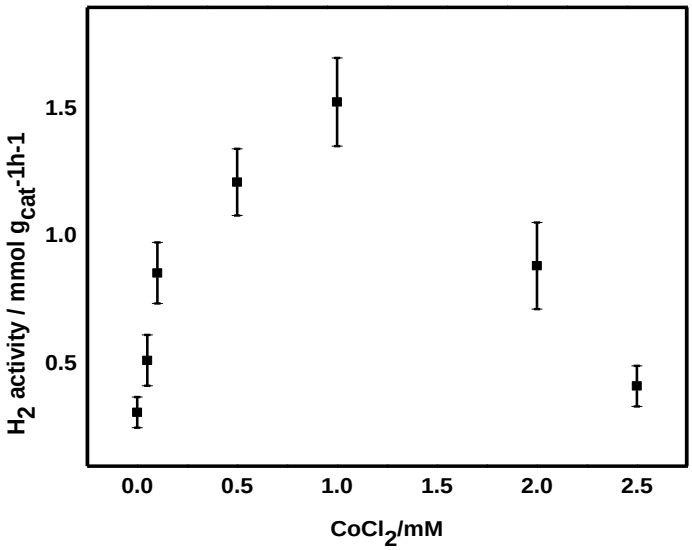

Figure 3.13 Photocatalytic H_2 generation using CdS/$CoCl_2$ at varying co-catalyst concentration (0.0 mM, 0.05 mM, 0.10 mM, 0.25 mM, 0.50 mM, 1.0 mM, 1.50 mM, 2.0 mM, and 2.50mM) [sunlight radiation; 185µM CdS (24µg mL^{-1}), 4.0 M $NaHCO_2$ in 2.0 mL formic acid; activity was determined after 1 h irradiation]

3.7.5(b) At varying co-catalyst concentration

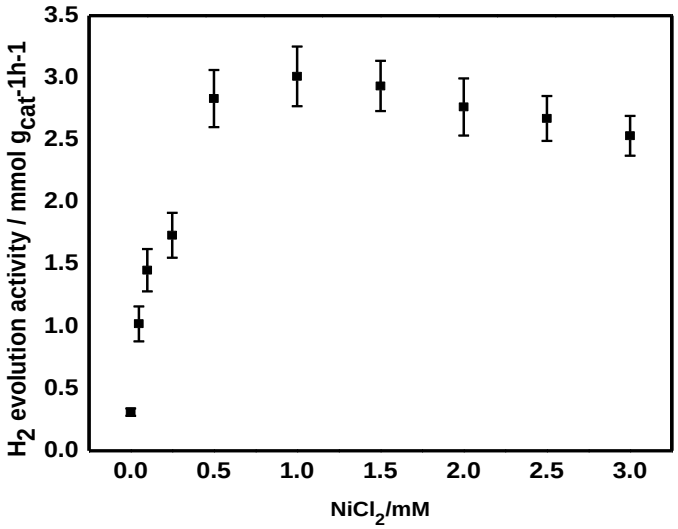

Figure 3.14 Photocatalytic H_2 generation using CdS/$NiCl_2$ at varying co-catalyst concentration (0.0mM, 0.05mM, 0.10mM, 0.25mM, 0.50mM, 1.0mM, 1.50mM, 2.0mM, and 2.50mM) [sunlight radiation; 185µM CdS (24µg mL^{-1}), 4.0 M $NaHCO_2$ in 2.0 mL formic acid; activity was determined after 1 h irradiation].

3.7.6. With and without addition of co-catalyst

The problem with CdS is its photoionstability which is due to photocorrosion of photogenerated holes (e.g. $CdS + 2h^+ \rightarrow Cd^{2+} + S^{2-}$). Photocatalyst in this case tend to be oxidized and result in blue shift because of Cd^{2+} [32, 33].This problem of photocatalyst might be overcome by loading with oxidation co-catalyst e.g. $CoCl_2.6H_2O$ **[shown in 3.6(b)].** By gradual oxidation of co-catalyst internally result in efficient removal of photogenerated holes from the photocatalyst and thus semiconductors are being sheltered from photo-oxidation. RuO_2 and CoOx on GaN:ZnO and TaON photocatalyst was found to be an effective way for improving the stability of photocatalyst in dehydrogenation process [34, 35]. In **Figure 3.15** hydrogen evolution increases after gradual interval of time because of the photostability of CdS semiconductor provided by loading with cobalt co-catalyst **(Supporting table 3.13).**

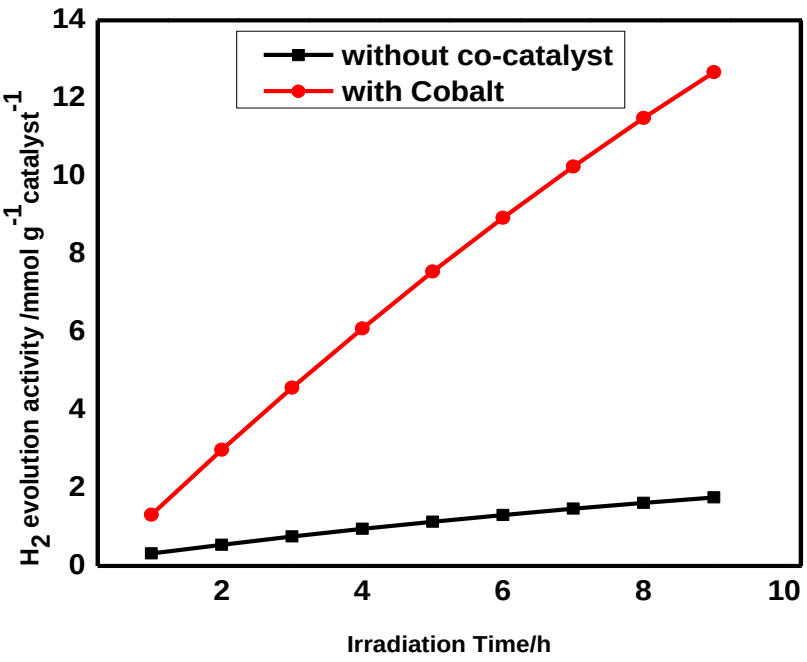

Figure 3.15 Photocatalytic H_2 generation with and without co-catalyst [sunlight radiation; 1mM $CoCl_2$, 4.0M $NaHCO_2$ in 2.0 mL formic acid; activity was determined after 1 h irradiation].

Continuously smaller blue shift **(Figure 3.16A)** on additional exposure to the acidic solution is due to the partial etching of naked CdS nanoparticle. Because of this etching

effect reduction in size of CdS nanoparticles takes place. As smaller particles have large surface area and thus absorb at smaller wavelength shows blue shift as compare to large particles. Optimum size and surface area are the need of efficient photocatalysis process, that's why size smaller than optimum has in turn decrease the photocatalytic process. Here the role of both co-catalyst to provide protection to the photocatalyst by keeping it shelter from the etching effect of acid as well as from photocorrosion of photogenerated holes **(Figure 3.16B).** Nickel provide protection from etching by coats on the surface of nanoparticles and cobalt shelter it from the photocorrosion, result in efficient removal of photogenerated holes from the semiconductor.

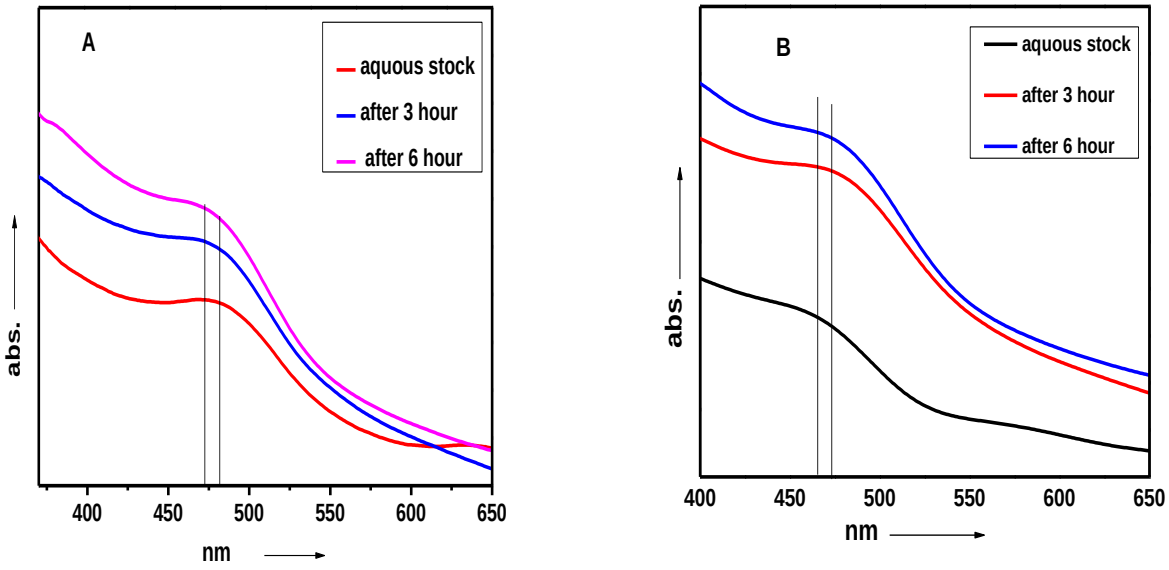

Figure 3.16 UV-Visible absorption spectra with and without addition of co-catalyst

3.7.7 Comparison of dual and individual co-catalysts

Loading of suitable dual co-catalyst on photocatalyst has been proved to be very efficient in increasing the photocatalytic activities of semiconductor **(Figure 3.17, 3.18).** Dual co-catalysts are necessary for developing highly efficient photocatalysts for photocatalytic hydrogen production [36, 37, 38]. Dual co-catalysts for reduction and oxidation was recently developed as an effective co-catalyst for the remedy of oxidation of CdS [39]. $CoCl_2.6H_2O$ as a oxidation co-catalyst and $NiCl_2.6H_2O$ as a reduction co-

catalyst have been used on CdS semiconductor and shows synergic effect just after 6 hour photocatalysis by efficiently increased in H_2 production . Loading of $NiCl_2$ on CdS as a reduction co-catalyst and $CoCl_2$ as an oxidation co-catalyst simultaneously, is supposed to be beneficial for effective suppression of electron-hole recombination. Single metal Ni and Co catalysts were also very effective, but it was observed after comparative study that they were inferior to Ni–Co catalyst, both in terms of conversions of formic acid and selectivity to the products [40]. The overall reaction rate is related to both oxidation and reduction reactions, so dealing well with both oxidation and reduction half reaction is equally important, but the slower one will be the rate determining step for the overall reaction [39]. After 6 hour dual Ni-Co on CdS semiconductor evolved 162 ±23 $mmolH_2g^{-1}$ while individual Ni and Co evolved upto 127±18 $mmolH_2g^{-1}$ and 83.9±11 $mmolH_2g^{-1}$ amount of hydrogen respectively (**Supporting table 3.10, 3.11 and 3.12)**

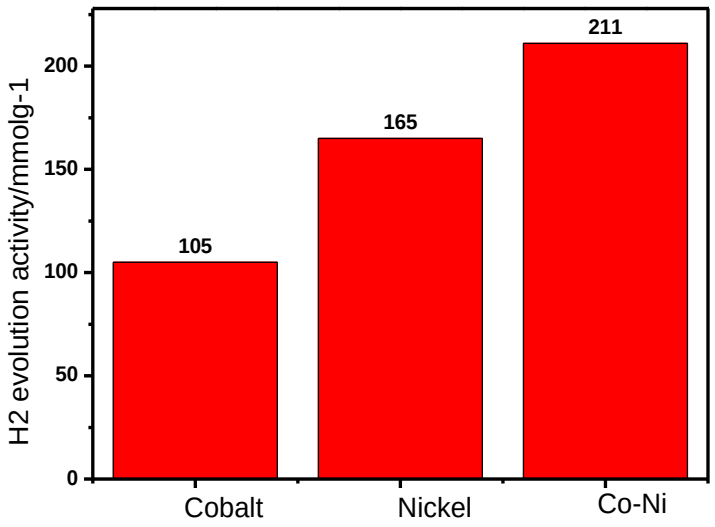

Figure 3.17 Comparison of different co-catalyst used for Hydrogen production after 12 hour photocatalysis

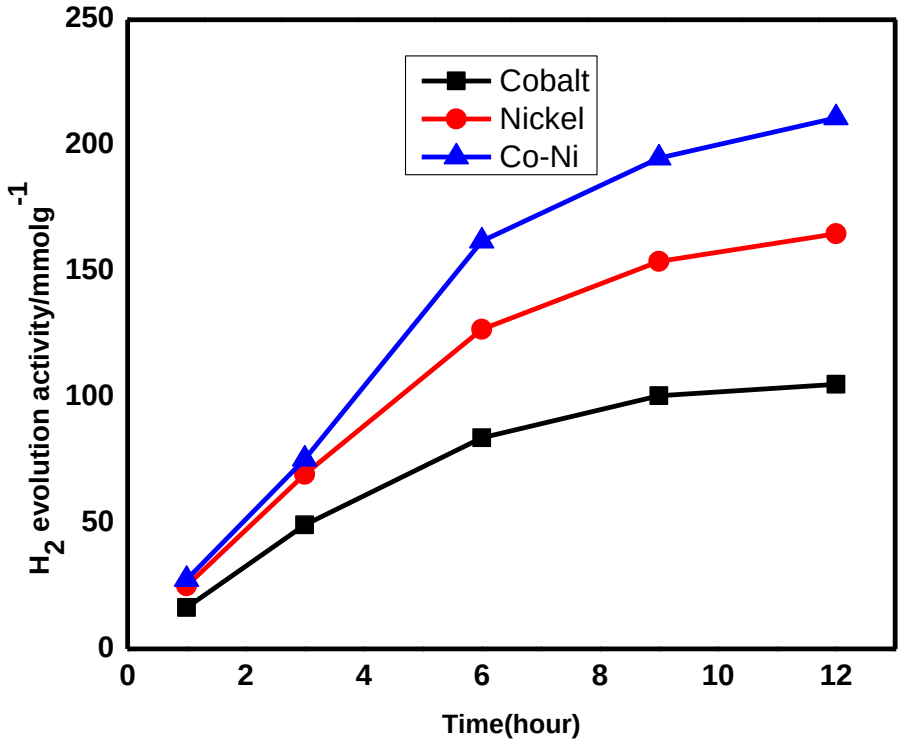

Figure 3.18. Comparison of H_2 formation rates for two common co-catalyst individually and then combinelly (dual). Sample was illuminated for 12 hours. Using 1mM CdS (150µg mL^{-1}, 100µL). The concentration of all precursors was 1mM, 4M $NaHCO_2$ in 2mL formic acid.

3.7.8. At varying light intensity

The activity of photocatalyst as well as rate of hydrogen production was continuously increases as soon as intensity of the trapped light enhanced **(Figure 3.19).** At 100 mW/Cm^2, 22 ±2.2$mmol/h^{-1}g^{-1}$ value of produced hydrogen was recorded, which shows the dependence of light intensity (no. of photons trapped on the semiconductor per unit area) on photocatalytic activity of photocatalyst. As number of photons trapped on the illuminated area of photocatalyst increases, the number of charge carrier also increases which in turn speed up the redox process **(Supporting table 3.16).**

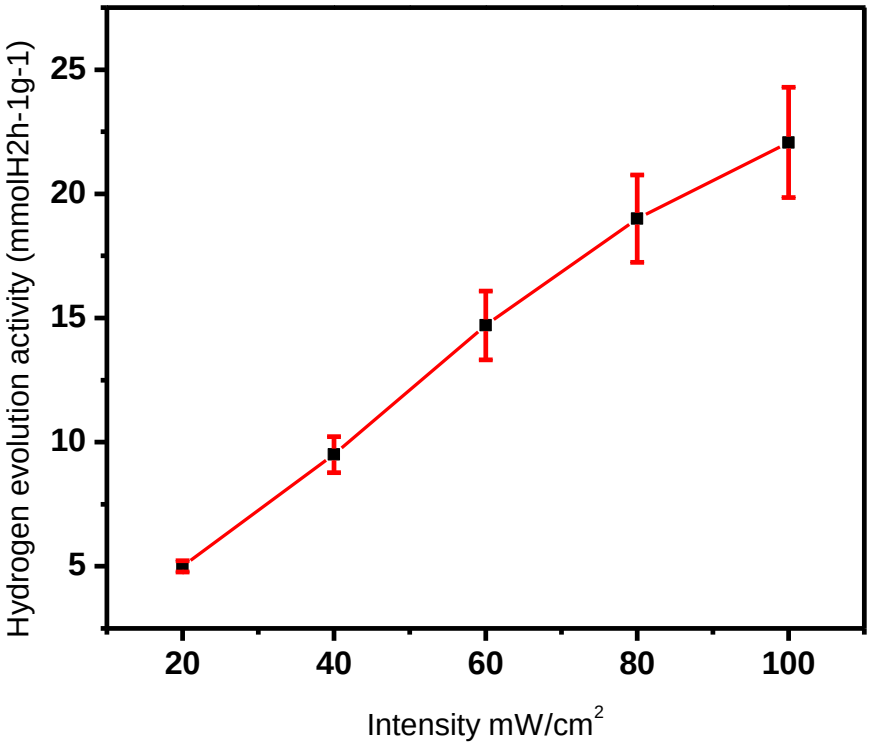

Figure 3.19 Photocatalytic H_2 generation using CdS/Co-Ni at varying light intensities AM1.5G, λ>420 nm, 0.5mM CdS (75µg mL^{-1}), 1mM $CoCl_2 \cdot 6H_2O$ and 1mM $NiCl_2.6H_2O$, 4.0 M $NaHCO_2$ in 2.0 mL formic acid. Activity was determined after 1 h irradiation.

3.7.9 Long term experiment for photocatalytic decomposition of formic acid using dual (Ni-Co) co-catalysts

Long term experiment for 12 hours was carried out to check the efficiency of CdS photocatalyst after loading with dual (Co-Ni) co-catalysts. Photocatalyst in the presence of this dual co-catalysts shown very appreciable and good photocatalytic activity **(Figure 3.20)**. 211 ±31mmol$H_2h^{-1}g^{-1}$ with 2028±14 turnover number was recorded after 12 hour photocatalysis **(Supporting table 3.12).**

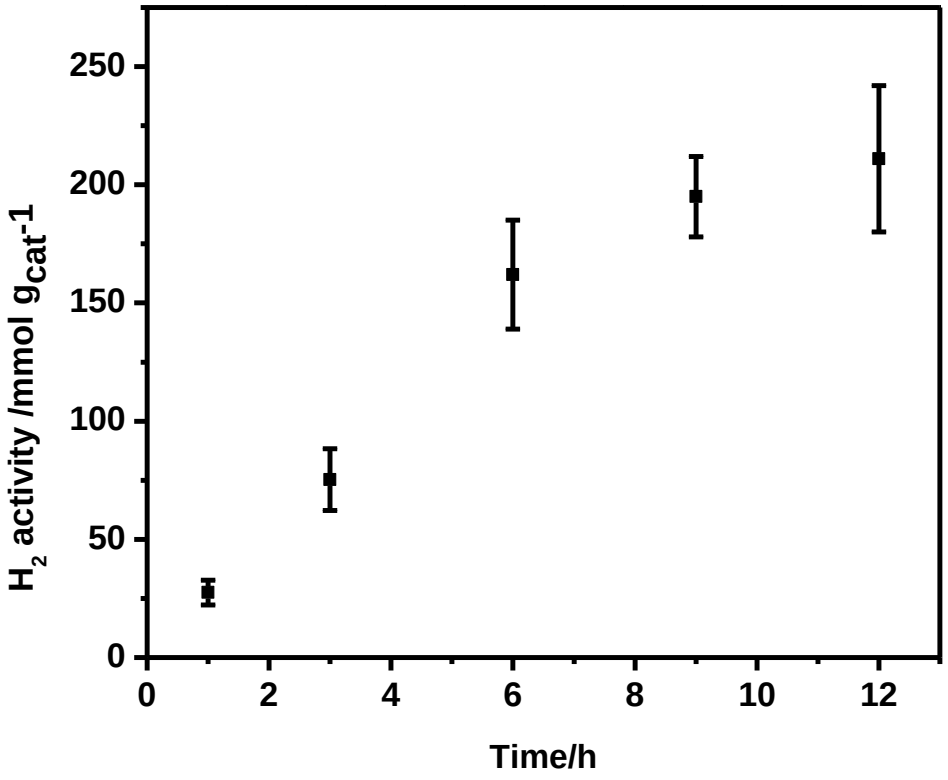

Figure 3.20 Photocatalytic H_2 generation using CdS/Co-$NiCl_2$, 1mM CdS (150µg mL^{-1},100µL), 1mM $CoCl_2 \cdot 6H_2O$, 4.0 M $NaHCO_2$ in 2.0 mL formic acid].

3.7.10 Long term experiment for photocatalytic decomposition of formic acid using cobalt as a co-catalyst

Long term experiment for 12 hours was carried out to check the efficiency of CdS photocatalyst after loading with Co^{+2} co-catalysts **(Figure 3.21).** Photocatalyst in the presence of this co-catalyst shown good photocatalytic activity as well as provide protection by this co-catalyst to the photocatalyst by efficiently withdraw photogenerated holes. $105\pm13 mmol H_2 h^{-1} g^{-1}$ with 1011±25 turnover number was recorded after 12 hour photocatalysis **(Supporting table 3.10).**

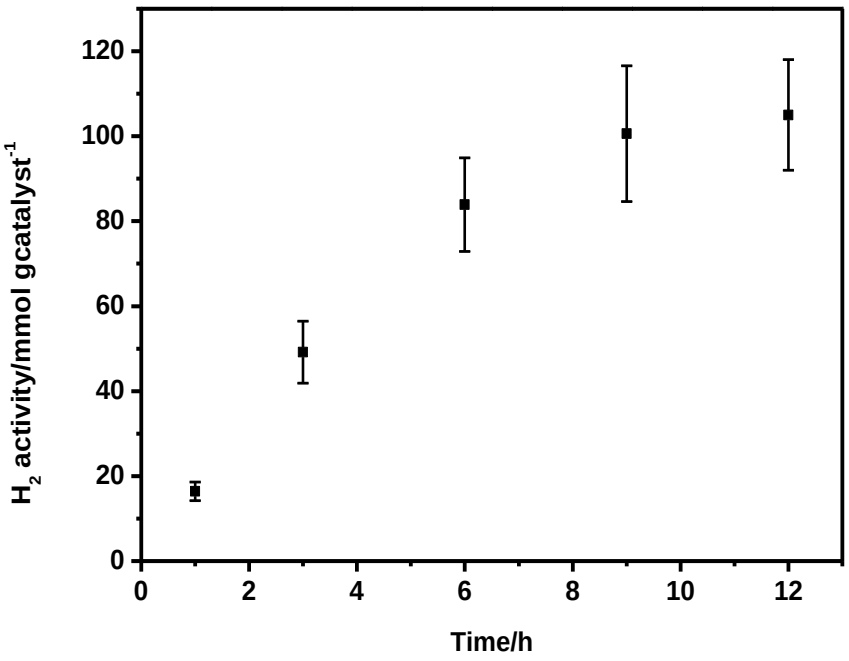

Figure 3.21 Photocatalytic H_2 generation using CdS/$CoCl_2$, 1mM CdS (150µg mL^{-1}, 100µL), 1mM $CoCl_2 \cdot 6H_2O$, 4.0 M $NaHCO_2$ in 2.0 mL formic acid].

3.7.11 Long term experiment for photocatalytic decomposition of formic acid using Nickel as a co-catalyst

Long term experiment for 12 hours was also carried out to check the efficiency of CdS photocatalyst after loading with Ni^{+2} co-catalysts **(Figure 3.22).** Photocatalyst in the presence of this co-catalysts shown better photocatalytic activity as well as provide protection by Ni^{+2} to this photocatalyst from the etching effect of acid after deposited on the surface of CdS semiconductor. 165 ±19 $mmolH_2h^{-1}g^{-1}$ with 1586±27 turnover number was recorded after 12 hour photocatalysis **(Supporting table 3.11).**

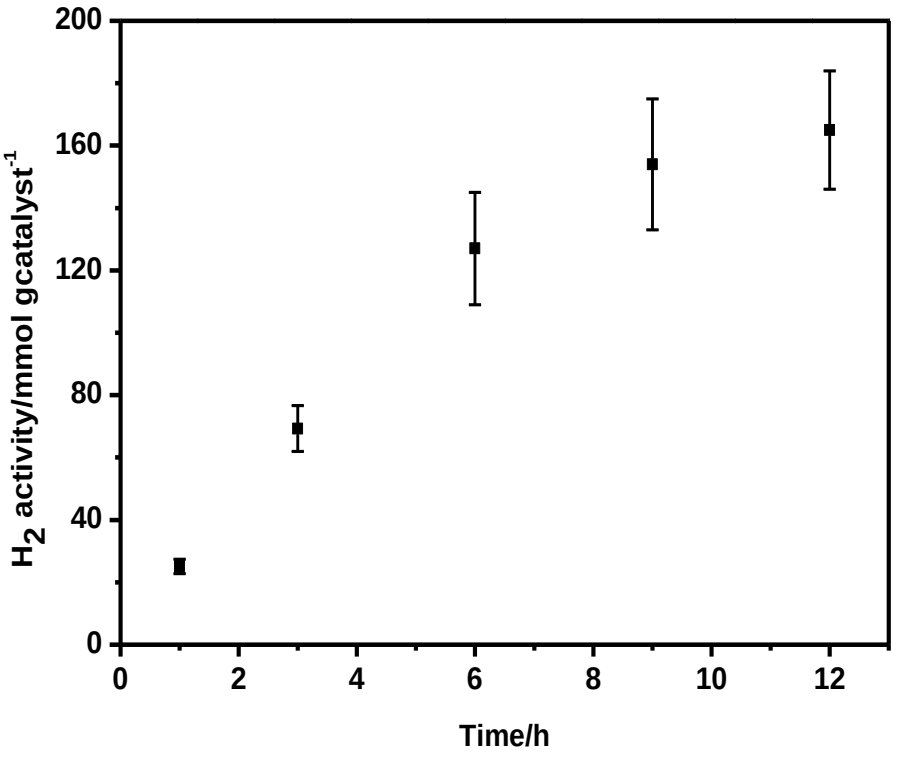

Figure 3.22. Photocatalytic H_2 generation using $CdS/NiCl_2$, 1mM CdS (150µg mL^{-1}, 100µL), 1mM $CoCl_2 \cdot 6H_2O$, 4.0 M $NaHCO_2$ in 2.0 mL formic acid].

.

3.8. Stability of the photocatalyst before and after photocatalysis

3.8.1 UV-Visible absorption spectra before and after 6 hour photocatalysis

Figure 3.23 clearly show bathochromic shift after photocatalysis. The 12 nm red shift and decrease in band gap of 0.3 eV indicate the aggregation of particles. Nanomaterial have large surface area and so tends to aggregate. Van der Waals forces compel these particles to aggregate, hence, result in red shift because of increase in size of particles.

There should be differentiation between aggregation and agglomeration. Agglomeration is when particles are joined loosely together which can be simply broken by mechanical forces but aggregation is a certain pattern of molecules which may be in any physical state. Aggregation phenomenon purely related to nanomaterial. The word "Particle" in the former case and the "Molecule" in the latter case should be in mind to differentiate these two terms.

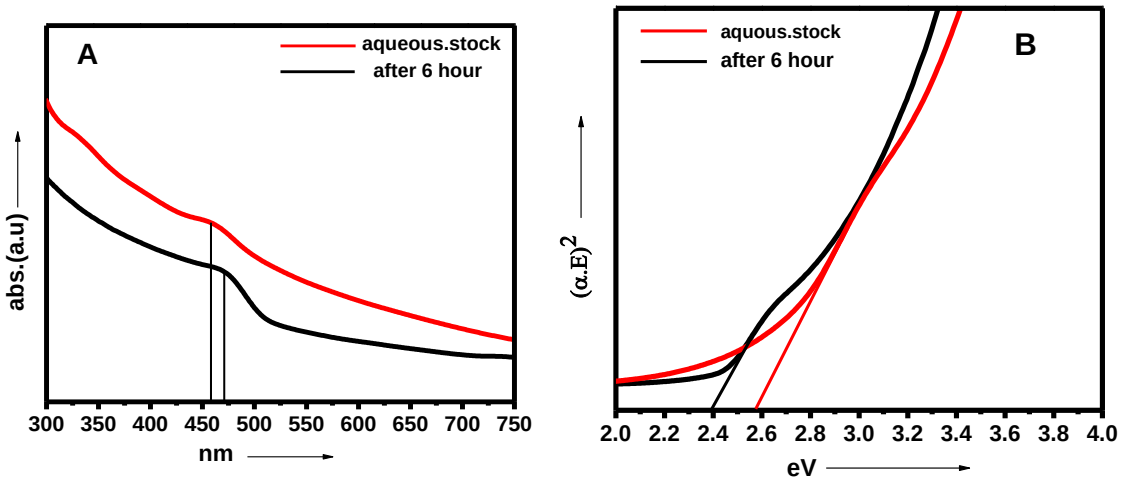

Figure 3.23. | UV-Vis absorption spectra of the CdS nanorods before and after 6 hour photocatalysis. A) Comparison of the absorption maxima spectra taken before and after the illumination. **B)** Band gap. The excitonic peak and energy band at respected position is denoted by the vertical lines.

3.8.2 SEM images before and after 6 hour photocatalysis

In **Figure 3.24** also confirm the aggregation of CdS nanoparticles. SEM image before photocatalysis scanned these particles to the average size of 29.5 nm, but after photocatalysis average size of 34.5 nm was recorded. Particles with very small size have large surface area tends to aggregate by mean of vander waals forces. Moreover, particles with smaller size, higher relative surface area, and higher relative numbers of surface atoms. Such surface atoms have unsaturated coordination (not complete coordination) and each atom has vacant coordination sites. A phenomenon so called dangling bonds. More bonds need to be formed per each surface atom. They try to make bonds, and such bonds tend to form between adjacent particles (bonds between surface atoms of each). It should also be noted that even for smaller size particles by sonication or other techniques, the small particles are still subject to agglomeration afterwards.

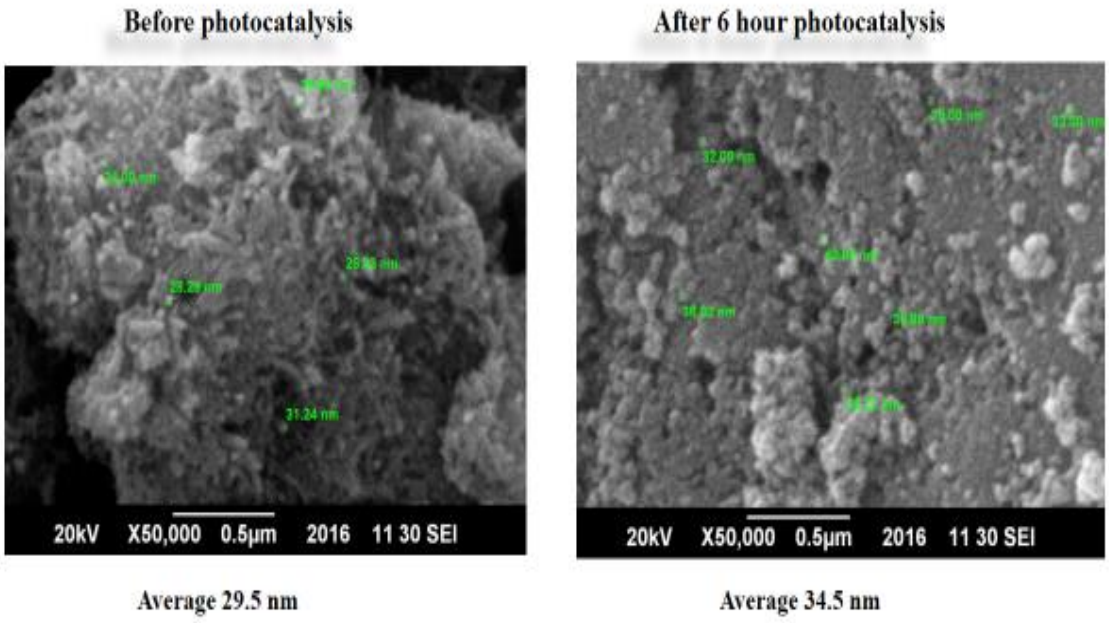

Figure 3.24 SEM images of CdS before and after 6 hour Photocatalysis

3.8.3 XRD spectra before and after 6 hour photocatalysis

For the used catalyst, there were no clear changes of the diffraction peaks. Based on these results we might conclude that no reconstruction of the sample took place during the process of photocatalysis. The structure of the photocatalyst was stable shown in **Figure 3.25,** which was in good agreements with the results of the characterized sample before photocatalysis [41].

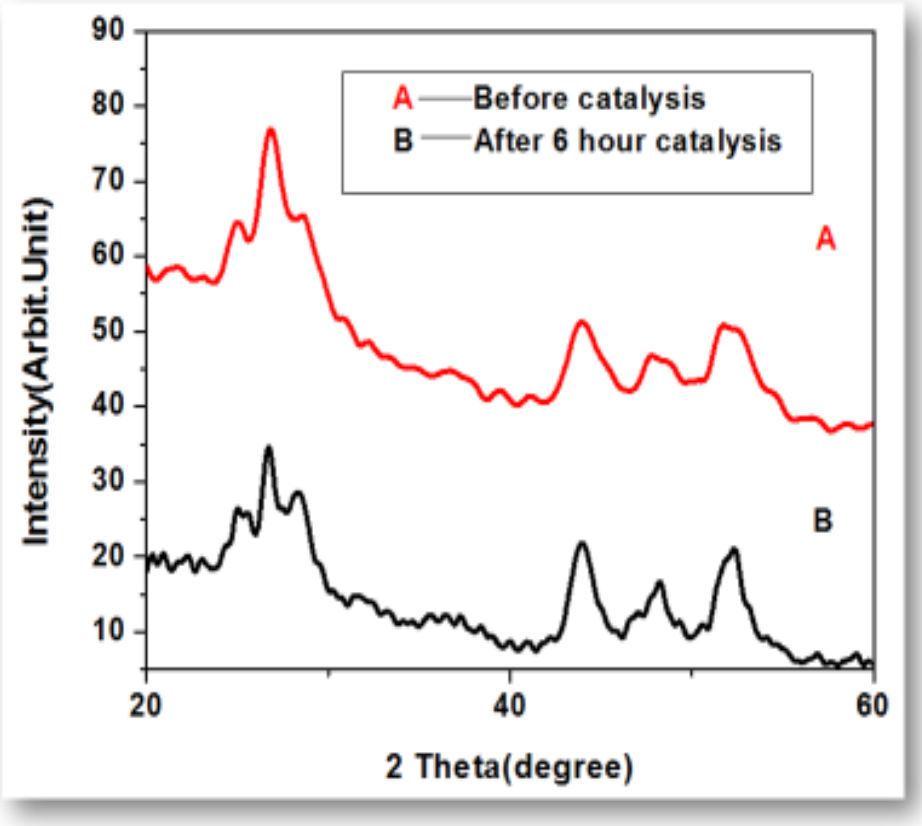

Figure 3.25 XRD Spectra of CdS before and after 6 hour Photocatalysis

3.8.4 EDX before and after 6 hour photocatalysis

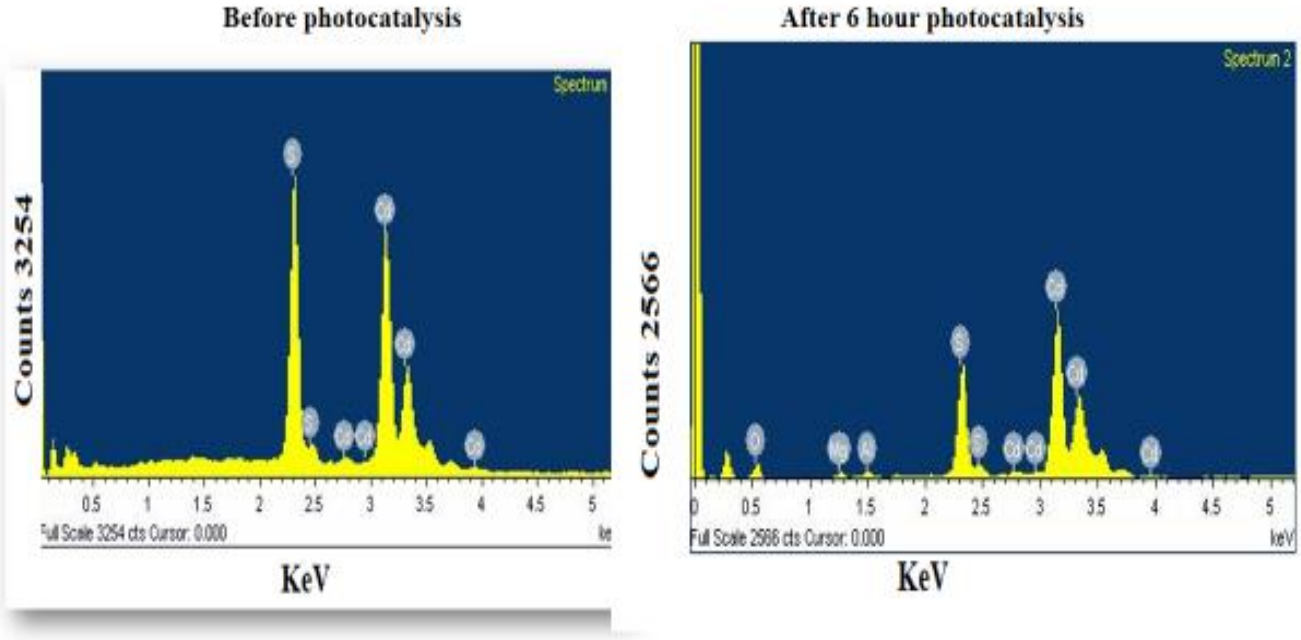

Figure 3.26 EDX Spectra of CdS before and after 6 hour Photocatalysis

Summary

CdS nanocrystals have been prepared without any capping agent under reflux condition by simple thermolysis using separately ethylenediamine and octylamine as a decomposing agents. All of these CdS nanoparticles have been characterized by UV-Visible, SEM, PXRD, FTIR and EDX. Small amount of $NiCl_2.6H_2O$ and $CoCl_2.6H_2O$ co-catalyst were loaded onto CdS photocatalyst that significantly improved the photocatalytic activity. The rate of H_2 evolution by the incorporation of MCl_2 onto CdS increases by a factor of approximately 5 as compared to that of the pure CdS. For complete suppression of electrons holes recombination dual co-catalyst were used. In summary, we have developed an inexpensive, highly active and selective dual co-catalyst system that leads to a substantial improvement in the photocatalytic generation of H_2 by the metal semiconductor, without the use of noble metal co-catalysts and protects the photocatalyst against photooxidation by complete suppression of electrons-holes recombination. By using aqueous dispersed solution of CdS and loading of dual co-catalyst onto the semiconductor shown almost 100% selectivity as well as synergism just after 6 hour photocatalysis.

This work provides an insight for designing Cadmium sulfide photocatalysts loaded by suitable co-catalyst onto the surface of this semiconductor, especially loading of dual co-catalyst with optimized reaction media, enables us to introduce novel flexibility in the sustainable use of formic acid as an energy source to generate efficient hydrogen.

References

1. Prakash, J. Thomas Joseph, and L. Ruby Nirmala. "Synthesis, spectral and thermal properties of bis thiourea zinc acetate (BTZA) single crystals."*Synthesis* 6.7 **(2010).**
2. Socrates, George. *Infrared and Raman characteristic group frequencies: tables and charts*. John Wiley & Sons, **2004**.
3. Acharya, K. P.: Photocurrent Spectroscopy of CdS/Plastic, CdS/Glass and ZnTe/GaAs Hetero-pairs Formed with Pulsed-Laser Deposition Ph.D. Thesis Bowling Green state University,**2009.**
4. Bandaranayake, R. J.; Wen, G. W.; Lin, J. Y.; Jiang, H. X.; Sorensen, C. M.: Structural Phase Behavior in II–VI Semiconductor Nanoparticles. *Applied Physics Lectures 1995,67,831-833.*
5. Singh, V.; Chauhan, P.: Synthesis and Structural Properties of Wurtzite Type CdS Nanoparticles *Chalcogenide Letters* **2009**, *6*, 421-426.
6. Pan, A.; Yang, H.; Liu, R.; Yu, R.; Zou, B.; Wang, Z.: Color-Tunable Photoluminescence of Alloyed CdSxSe1-x Nanobelts *Journal of the American Chemical Society* **2005**, *127*, 15692-15693.
7. Thongtem, T.; Phuruangrat, A.; Thongtem, S.: Solvothermal Synthesis of CdS Nanowires Templated by Polyethylene Glycol. *Ceramics International***2009**, 35, 2817-2822.
8. Singh, V.; Chauhan, P.: Synthesis and Structural Properties of Wurtzite Type CdS Nanoparticles. *Chalcogenide Letters* **2009**, *6*, 421-426.
9. Banerjee, R.; Jayakrishnan, R.; Ayyub, P.: Effect of the Size-Induced Structural Transformation on the Band Gap in CdS Nanoparticles. *Journal of Physics: Condensed Matter2000, 12,*10647-10654.
10. A S Vorokh; A A Rempel: Atomic Structure of Cadmium Sulfide Nanoparticles. *Physics of the Solid State* **2007**, *49*, 148-153.
11. G. K. Sandhu, N. S. Boparoy, Synth. React. Met.–Org. Chem., 20, 975 (**1990**)
12. O. Jung, Y. S. Sohn, J. A. Ibers, *Inorg. Chem.*, 2273, 25 (**1986**).
13. B Srinivasa Rao; B Rajesh Kumar; V Rajagopal Reddy; T Subba Rao; G Venkat *Chalgogenide Letters* **2011**, *8*, 39-44

14. Bao, Ningzhong, et al. "Self-templated synthesis of nanoporous CdS nanostructures for highly efficient photocatalytic hydrogen production under visible light.“*Chemistry of Materials* 20.1 (2007): 110-117

15. Hill, S. P., and J. M. Winterbottom. "The conversion of polysaccharides to hydrogen gas. Part I: The palladium catalysed decomposition of formic acid/sodium formate solutions." *Journal of Chemical Technology and Biotechnology* 41.2 (1988): 121-133.

16. Wang, Zhi-Li, et al. "Pd/C synthesized with citric acid: an efficient catalyst for hydrogen generation from formic acid/sodium formate." ." *Scientific reports* 2 (2012).

17. Zhou, Xiaochun, et al. "High-quality hydrogen from the catalyzed decomposition of formic acid by by Pd–Au/C and Pd–Ag/C ." *Chemical Communications* 30 (2008) 3540-3542.

18. Ojeda, Manuel, and Enrique Iglesia. "Formic Acid Dehydrogenation on Au-Based Catalysts at Near-Ambient Temperatures." *Angewandte Chemie*121.26 (2009): 4894-4897.

19. Gu. Xiaojun, et al. "Synergistic catalysis of metal–organic framework-immobilized Au–Pd nanoparticles in dehydrogenation of formic acid for chemical hydrogen storage." *Journal of the American Chemical Society*133.31 (2011): 11822-11825.

20. Bi, Qing-Yuan, et al. "Efficient subnanometric gold-catalyzed hydrogen generation via formic acid decomposition under ambient conditions." *Journal of the American Chemical Society* 134.21 (2012): 8926-8933.

21. Bao, Ningzhong, et al. "Self-templated synthesis of nanoporous CdS nanostructures for highly efficient photocatalytic hydrogen production under visible light." *Chemistry of Materials* 20.1 (2007): 110-117.

22. Ling, Feng, et al. "PdO/LaCoO 3 heterojunction photocatalysts for highly hydrogen production from formaldehyde aqueous solution under visible light."*International Journal of Hydrogen Energy* (2015).

23. Sasaki, Yasuyoshi, et al. "The effect of co-catalyst for Z-scheme photocatalysis systems with an $Fe^{3+/}Fe^{2+}$ electron mediator on overall water splitting under visible light irradiation." *Journal of Catalysis* 259.1 (2008): 133-137.

24. Simon, Thomas, et al. "Redox shuttle mechanism enhances photocatalytic H^2 generation on Ni-decorated CdS nanorods." *Nature materials* 13.11 (2014): 1013-1018.

25. Hydrogen: The Wonderful Fuel by T.N.Veziroglu F.berbir

26. Kuehnel, Moritz F., et al. "Photocatalytic Formic Acid Conversion on CdS Nanocrystals with Controllable Selectivity for H2 or CO." *Angewandte Chemie International Edition* 54.33 (2015): 9627-9631.

27. Kuehnel, Moritz F., et al. "Photocatalytic Formic Acid Conversion on CdS Nanocrystals with Controllable Selectivity for H_2 or CO." *Angewandte Chemie International Edition* 54.33 (2015): 9627-9631.

28. Willner I, Goren Z. J. Chem. Soc. Chem. Commun. 1986:172–173.

29. Bao, Ningzhong, et al. "Self-templated synthesis of nanoporous CdS nanostructures for highly efficient photocatalytic hydrogen production under visible light." *Chemistry of Materials* 20.1 (2007): 110-117.

30. Yang, Jinhui, et al. "Roles of cocatalysts in photocatalysis and photoelectrocatalysis." *Accounts of chemical research* 46.8 (2013): 1900-1909.

31. Higashi, Masanobu, Kazunari Domen, and Ryu Abe. "Highly stable water splitting on oxynitride TaON photoanode system under visible light irradiation." *Journal of the American Chemical Society* 134.16 (2012): 6968-6971.

32. Ohno, Tomoyuki, et al. "Photocatalytic water splitting using modified GaN: ZnO solid solution under visible light: long-time operation and regeneration of activity." *Journal of the American Chemical Society* 134.19 (2012): 8254-8259.

33. Ma, Baojun, et al. "The synergistic effects of two co-catalysts on Zn2GeO4 on photocatalytic water splitting." *Catalysis letters* 134.1-2 (2010): 78-86.

34. Maeda, Kazuhiko, et al. "Photocatalytic overall water splitting promoted by two different cocatalysts for hydrogen and oxygen evolution under visible light." *Angewandte Chemie* 122.24 (2010): 4190-4193.

35. 林峰, et al. "Photocatalytic oxidation of thiophene on $BiVO_4$ with dual co-catalysts Pt and RuO_2 under visible light irradiation." (2012).

36. Yang, Jinhui, et al. "Roles of cocatalysts in photocatalysis and photoelectrocatalysis." *Accounts of chemical research* 46.8 (2013): 1900-1909.

37. Hu, Xun, and Gongxuan Lu. "Investigation of steam reforming of acetic acid to hydrogen over Ni–Co

38. Jang, Jum Suk, Upendra A. Joshi, and Jae Sung Lee. "Solvothermal synthesis of CdS nanowires for photocatalytic hydrogen and electricity production." *The Journal of Physical Chemistry C* 111.35 (2007): 13280-13287.

Supporting tables

Table 3.7 Photocatalytic H_2 generation using CdS/$CoCl_2$ at varying CdS concentration [sunlight radiation; 1mM $CoCl_2$, 4.0M $NaHCO_2$ in 2.0 mL formic acid; activity was determined after 1 h irradiation]. Data is given as mean ±s.d. of two independent measurements

Entry	c(CdS)aquaous dispersed) /uM	H_2 activity±σ[a] /mmol H_2 $gcatalyst^{-1}h^{-1}$	TON ±σ[b] /mol H_2 mol_{cds}^{-1}
1[b]	170	0.513 ±0.32	227 ±7.0
2	185	1.159 ±0.8	323 ±12
3	200	1.946 ±0.7	512 ±10
4	215	2.353 ±0.9	573 ±15
5	230	2.531 ±1.1	575 ±21
6	260	2.816 ±1.3	599 ±17

[a]Calculated using the mass of CdS + $CoCl_2.6H_2O$, nμM of CdS (n=170,185 etc. 20μL) [b] TON_{cds} = nH2/nCdS

Table 3.8 Photocatalytic decomposition of sodium formate (SF/FA) using CdS at varying formate concentrations [185μM bulk CdS (24μg mL^{-1}), 1mM $CoCl_2.6H_2O$ in 2.0 ml formic acid, pH not adjusted. Activity was determined after 1 h irradiation]. Data is given as mean ±s.d. of two independent measurements].

Entry	c($NaHCO_2$) /M	H_2activity $\pm\sigma^{[a]}$/mmolH_2 $g_{catalys}^{-1}h^{-1}$	TON ± $\sigma^{[b]}$ /mol H_2 mol_{cds}^{-1}
1	0.5	0.177±0.04	50 ±3.2
2	1.0	0.494±0.04	141 ±8.8
3	1.5	0.552±0.05	157 ±6.7
4	2.0	0.593±0.06	170 ±13
5	2.5	0.646±0.07	184 ±11
6	3.0	0.831±0.09	237 ±10
7	4.0	0.845±0.11	240±11
8	5.0	0.839±0.10	238 ±12

[a]Calculated using the mass of CdS + $CoCl_2.6H_2O$, CdS 85μM (24μg mL^{-1}, 20μL) [b] TON_{cds} = nH_2/nCdS

Table 3.9 Photocatalytic H_2 generation using $CdS/CoCl_2$ at varying co-catalyst concentration [sunlight radiation; 185μM CdS (24μg mL^{-1}), 4.0 M $NaHCO_2$ in 2.mL formic acid; activity was determined after 1 h irradiation]. Data is given as mean ±s.d. of two independent measurements]

Entry	$c(CoCl_2.6H_2O)$ /mM	H_2 activity±[a]σ /mmol $g_{catalyst}^{-1}h^{-1}$	TON [b]σ ± /mol H_2 mol_{CdS}^{-1}
1	0.0	0.311 ±0.06	89 ±8.30
2	0.05	0.515 ±0.10	147 ±11.5
3	0.10	0.858 ±0.12	245 ±9.30
4	0.25	0.907 ±0.13	259 ±5.50
5	0.50	1.214 ±0.13	347 ±13.0
6	1.00	1.529 ±0.17	437 ±10.0
7	1.50	0.843 ±0.54	241 ±12.5
8	2.00	0.886 ±0.17	254 ±7.50
9	2.50	0.414 ±0.08	118 ±5.50

[a]Calculated using the mass of CdS + $CoCl_2.6H_2O$ 185μM CdS (24 μg mL^{-1}, 20μL) [b] TON_{cds} = $nH_2/nCdS$

Table 3.10 Photocatalytic H_2 generation from formic acid/sodium formate using CdS/$CoCl_2$ 1mM CdS (150μgmL^{-1}), 1mM $CoCl_2 \cdot 6H_2O$, 4.0M $NaHCO_2$ in 2.0 mL formic acid. Data is given as mean ±s.d. of two independent measurements].

Entry	Time /h	H_2activity±σ[a] /mmol $g_{catalyst}^{-1}$	TON σ ±[b] /mol H_2 mol_{CdS}^{-1}
1	1	16.4 ±2.2	157±12
2	3	49.2 ±7.3	473±15
3	6	83.9 ±11	806±18
4	9	100.6 ±16	967±22
5	12	105 ±13	1011±25

[a] Calculated using the mass of CdS + $CoCl_2.6H_2O$ CdS 1mM (150μg mL^{-1}, 100μL) [b] $TON_{cds} = nH_2/nCdS$

Table 3.11 Photocatalytic H_2 generation from formic acid/sodium formate using CdS/$NiCl_2$ 1mM CdS (150μgmL^{-1}), 1mM $NiCL_2 \cdot 6H_2O$, 4.0M $NaHCO_2$ in 2.0 mL formic acid. Data is given as mean ±s.d. of two independent measurements].

Entry	Time /h	H_2activity±σ[a] /mmol $g_{catalyst}^{-1}$	TON σ ±[b] /mol H_2 mol_{CdS}^{-1}
1	1	25.1±2.3	241±14
2	3	69.3±7.3	666±17
3	6	127±18	1221±27
4	9	154 ±21	1480±29
5	12	165 ±19	1586±27

[a]Calculated using the mass of CdS + $NiCl_2.6H_2O$ 1mM CdS (150 μg mL^{-1}, 100μL) [b] TON_{cds} = nH_2/nCdS

Table 3.12 Photocatalytic H_2 generation from formic acid/sodium formate using CdS/Ni-Co 1mM CdS (150μgmL^{-1}), 1mM both $NiCL_2 \cdot 6H_2O$ and $CoCl_2.6H_2O$, 4.0M $NaHCO_2$ in 2.0 mL formic acid. Data is given as mean ±s.d. of two independent measurements].

Entry	Time /h	H_2activity±σ[a] /mmol $g_{catalyst}^{-1}$	TON σ ±[b] /mol H_2 mol_{CdS}^{-1}
1	1	27.5 ±5.1	267±17
2	3	75.3 ±13	724±14
3	6	162 ±23	1557±14
4	9	195 ±17	1875±14
5	12	211 ±31	2028±14

[a]Calculated using the mass of CdS + $NiCl_2$ /$CoCl_2$ (CdS 150 μg mL^{-1}, 100μL) [b] TON_{cds} = nH_2/nCdS

Table 3.13 Photocatalytic H_2 generation with and without Co-catalyst [sunlight radiation; 1mM $CoCl_2$, 4.0M $NaHCO_2$ in 2.0 mL formic acid; activity was determined after 1h irradiation]. Data is given as mean ±s.d. of two independent measurements.

Entry	Time/h	Without cocatalyst/mmolH_2 $g_{catalyst}^{-1}h^{-1}$[a]	With $CoCl_2$/ mmol$H_2g_{catalyst}^{-1}h^{-1}$[a]
1[b]	1	0.311±041	1.52 ±0.14
2	2	0.571±062	2.87±0.28
3	3	0.788±052	4.07±0.17
4	4	0.939±071	6.23±0.54
5	5	1.034±078	7.98±0.57
6	6	1.281±045	8.99±0.21
7	7	1.577±069	10.1±0.43
8	8	1.671±078	11.3±0.58
9	9	1.694±089	12.7±0.60

[a]Calculated using the mass of CdS + $CoCl_2.6H_2O$, CdS 185µM (24µg mL^{-1}, 20µL)

Table 3.14 Photocatalytic H_2 generation using $CdS/NiCl_2$ at varying co-catalyst concentration [sunlight radiation; 185μM CdS (24μg mL^{-1}), 4.0 M $NaHCO_2$ in 2mL formic acid; activity was determined after 1 h irradiation]. Data is given as mean ±s.d. of two independent measurements]

Entry	**$NiCl_2.6H_2O$/mM**	**H_2activity±σ[a] /mmol $g_{catalyst}^{-1}h^{-1}$**	**TON ± σ[b] /mol H_2 mol_{cds}^{-1}**
1	0	0.311	89
2	0.05	1.021	292
3	0.1	1.453	415
4	0.25	1.734	496
5	0.5	2.834	811
6	1	3.012	861
7	1.5	2.934	839
8	2	2.765	791
9	2.5	2.673	764
10	3	2.534	725

[a] Calculated using the mass of CdS + $NiCl_2.6H_2O$, 185μM CdS (24μg mL^{-1}, 20μL) [b] TON_{cds} = $nH_2/nCdS$

Table 3.15 External quantum yield determination for the photocatalytic H_2 generation from formic acid/sodium formate using CdS/Ni-Co [I= 40mW cm^{-2}, λ=460±10nm, A=3.15 cm^2; 1mM (150μg mL^{-1}), 0.5mM $CoCl_2 \cdot 6H_2O$, 4.0 M $NaHCO_2$ in 2.0 mL formic acid.

Entry	**Time /h**	**nH_2 ±/μmol**	**EQY_{H2} / %**
1	1	0.0270	15.75
2	2	0.0276	16.02
3	3	0.0242	13.85
4	4	0.0211	12.08
5	5	0.0371	21.72
6	6	0.0241	13.73
Average		0.0268	15.52

Formula for the determination of external quantum yield (EQY).

Formula = $100\% \times \frac{2 \times n\mathbf{H_2} \times NA \times h \times c}{tirr \times \lambda \times I \times A}$

Where $n\mathbf{H_2}$ is the amount of H_2 generated

N_A is Avogadro's constant

H is Planck's constant

c is the speed of light

t_{irr} is the irradiation time

λ is the wavelength

I is the light intensity

A is the irradiated area of the photoreactor

Table 3.16 Photocatalytic H_2 generation using CdS/Co-Ni at varying light intensities, AM 1.5G λ>420 nm, 0.25mM CdS (37.5μg mL^{-1}), 1mM $CoCl_2 \cdot 6H_2O$ and 1mM $NiCl_2.6H_2O$, 4.0 M $NaHCO_2$ in 2.0 mL formic acid. Activity was determined after 1 h irradiation.

Entry	Intensity /$mWcm^{-2}$	H_2activity±σ /mmol $g_{catalyst}^{-1}$	EQY_{H2} / %
1	20	5 ±0.23	5.04
2	40	9.5 ±0.73	5.23
3	60	14 ±1.3	4.65
4	80	19 ±1.7	4.71
5	100	22 ±2.2	4.42